ISSN 1666-115X

Boletín del Instituto de Fisiografía y Geología

Volúmen 78 (2008), Números 1-2

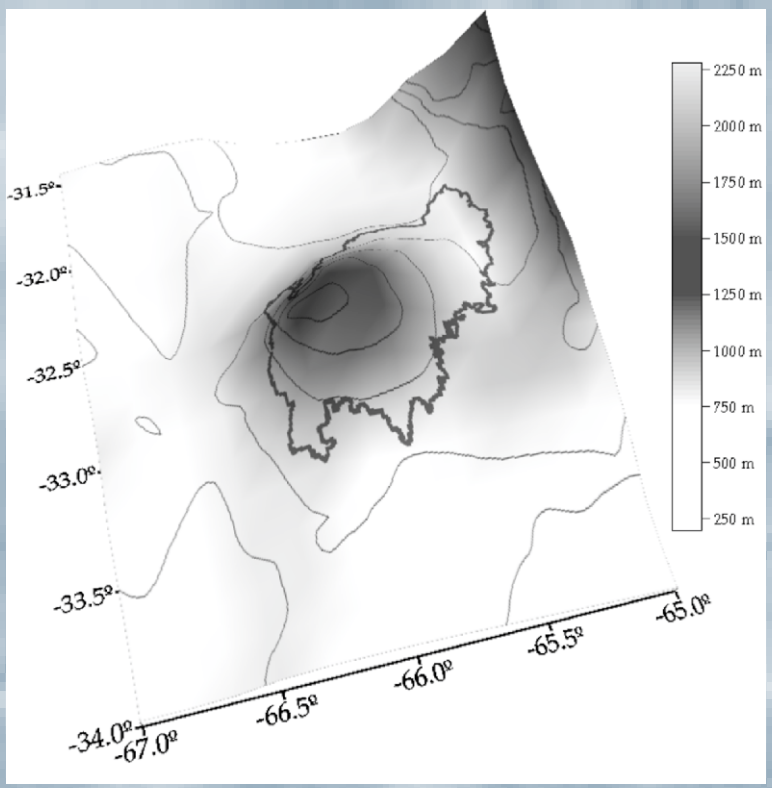

Rosario, Diciembre 2008

Boletín del Instituto de Fisiografía y Geología

ISSN 1666-115X

Edición del Instituto de Fisiografía y Geología
"Dr. Alfredo Castellanos"
Facultad de Ciencias Exactas, Ingeniería y Agrimensura
Universidad Nacional de Rosario
Pellegrini 250, 2000 Rosario, Argentina

E-mail: ifg@fceia.unr.edu.ar

URL: http://www.fceia.unr.edu.ar/fisiografia

Características y alcance

El Boletín IFG es una revista internacional de publicación periódica de artículos científicos originales sobre temas de las denominadas Ciencias de la Tierra (Geología, Estratigrafía, Paleontología, y disciplinas afines), cuyos tópicos estén o no incluídos en los campos de investigación del Instituto de Fisiografía y Geología. Sólo son aceptados manuscritos de trabajos inéditos consistentes en contribuciones científicas significativas a criterio de los Editores y los árbitros. Todos los manuscritos son sometidos a arbitraje internacional de por, al menos, dos reconocidos especialistas en la materia. La decisión final de aceptación de un manuscrito para su publicación es de los Editores.

Ediciones anteriores

El Boletín IFG es la serie única que reemplaza y sucede todas las ediciones anteriores del Instituto de Fisiografía y Geología que se publicaron con los nombres "Publicaciones" [ISSN 0041-8684], "Notas A" [ISSN 0325-4100] y "Notas B" [ISSN 0326-470X]. La numeración de la nueva y única serie comienza en el Volúmen 70, correlativo con el último número de la antigua serie principal "Publicaciones", finalizada en 1996 con el número 69. Se publicará un volumen anual, dividido en un número variable de fascículos que dependerá de la extensión y número de contribuciones que se incluyan.

Suscripción e intercambio

El Boletín IFG puede obtenerse por intercambio institucional, suscripción individual o suscripción institucional, dirigiéndose a la dirección indicada arriba. La nómina de los números anteriores disponibles puede obtenerse del sitio de internet indicado arriba, así como todos los números anteriores disponibles en formato pdf.

Aim and scope

The Boletín IFG is an international periodical journal containing original scientific articles on the so called Earth Sciences (Geology, Stratigraphy, Paleontology, and related matters), related or not with the fields or research of the Instituto de Fisiografía y Geología. Only are acepted manuscripts of unpublished results consisting of significant scientific contributions. Every manuscript is subject to international peer review by at least two reviewers or referees, well known specialists on the matter. Final decision of publication is of the Editors.

Past editions

The Boletín IFG is the unique series of publications which replace and follows any former and past editions of the Instituto de Fisiografía y Geología which were published under the following names: "Publicaciones" [ISSN 0041-8684], "Notas A" [ISSN 0325-4100] y "Notas B" [ISSN 0326-470X]. The first volume of the series is the volume 70 correlative with the last of the former series "Publicaciones", ended in 1996 with the number 69. It will be published one single volume per year, subdivided in a number of fascicules depending on the number and size of contributions included.

Suscription and exchange

The Boletín IFG can be obtained by institutional exchange, individual suscription or institutional suscription contacting to the adresses given above. All current and past publications are free available on-line in the website cited above, in pdf format.

Portada: Topograía suavizada de la Sierra de San Luis, Argentina. [Figura 12 en Cornaglia & Introcaso, este volúmen]

ALTERNATIVE GRAVIMETRIC METHODOLOGY FOR ISOSTATIC ANALYSES. AN EXAMPLE FOR BOLIVIAN ANDES

Carolina B. CROVETTO & Antonio INTROCASO

Boletín del Instituto de Fisiografía y Geología

Crovetto C.B. & Introcaso A., 2008. Alternative gravimetric methodology for isostatic analyses. An example for Bolivian Andes. *Boletín del Instituto de Fisiografía y Geología* **78(1-2)**: 1-12. Rosario, 02-12-2008. ISSN 1666-115X.

Abstract.- In this work we present a new, alternative methodology for performing isostatic studies by means of geoid undulations, excluding the use of measured gravity anomalies. An example on Bolivian Andes is presented as case study. Considering a digital elevation model as input data, a theoretical perfectly isostatically balanced Airy crustal model was constructed for Bolivia. The free-air and the Bouguer anomalies, and the geoid undulations produced by this theoretical model, were directly evaluated by means of three-dimensional integration. The "real" geoid undulations were computed from the EGM96 global geopotential model, and were filtered from long wavelengths by means of a sparse Fourier transform method. The residual "real" geoid undulations were compared with the theoretical geoid undulations for Bolivian Andes, showing a global tendency towards isostatic balance, agreeing with previous results obtained using traditional gravimetry.

The free-air and the Bouguer anomalies from the EGM96 residual geoid undulations were also evaluated and then compared with the anomalies produced by the theoretical model. The Bouguer anomalies support definitely the results obtained using the geoid undulations while the free-air anomalies, although less consistently, showed the same global tendency.

Key-words: Geoid; Gravity anomalies; Isostasy; New methodology; Bolivian Andes.

Resumen.- ***Método gravimétrico alternativo para análisis isostáticos. Ejemplo sobre los Andes Bolivianos.*** En este trabajo presentamos una nueva metodología alternativa para realizar estudios isostáticos empleando ondulaciones del geoide, sin utilizar anomalías de gravedad observadas. Un ejemplo sobre los Andes Bolivianos se presenta como caso de estudio. Considerando un modelo digital de elevación como dato de entrada, se construyó un modelo cortical teórico perfectamente balanceado siguiendo la hipótesis de Airy para Bolivia. Las anomalías de aire libre y de Bouguer, y las ondulaciones del geoide producidas por dicho modelo teórico se evaluaron directamente mediante integraciones en tres dimensiones. Las ondulaciones del geoide "reales" se obtuvieron a partir del modelo geopotencial global EGM96, de las cuales se filtraron las largas longitudes de onda mediante el empleo de una transformada de Fourier rala. Las ondulaciones del geoide "residuales" fueron comparadas con las ondulaciones teóricas en los Andes Bolivianos, mostrando una tendencia general al equilibrio isostático, en total acuerdo con los resultados gravimétricos previos.

Se evaluaron también las anomalías de aire libre y de Bouguer a partir de las ondulaciones del geoide residuales derivadas del EGM96, las cuales se compararon con las anomalías de gravedad generadas por el modelo teórico. Las anomalías de Bouguer certificaron definitivamente el resultado encontrado empleando el geoide, y las anomalías de aire libre, si bien resultaron menos consistentes, mostraron la misma tendencia global.

Palabras clave: Geoide; Anomalías de gravedad; Isostasia; Nueva metodología; Andes Bolivianos.

Carolina Beatriz Crovetto [e-mail: carolina@crovetto.com]: *Grupo de Geofísica, Instituto de Física Rosario, Av. Pellergini 250, Rosario, Argentina.*

Antonio Introcaso [e-mail: geofisic@fceia.unr.edu.ar]: *Grupo de Geofísica, Instituto de Física Rosario (CONICET – UNR), Av. Pellegrini 250, Rosario, Argentina.* [Correspondence author].

Digital Supplementary Material / Material Suplementario Digital (MSD): http://www.fceia.unr.edu.ar/fisiografia.

Received: 15/04/2008; accepted: 15/08/2008.

INTRODUCTION

Isostasy studies the equilibrium of the crust and the lithosphere of the Earth. Isostatic balance is usually analysed employing isostatic anomalies, derived from measured gravity values. These anomalies are compared with those produced by a balanced model, assuming different isostatic hypothesis (Airy 1855, Pratt 1855, Vening Meinesz 1931).

In this work we propose a new alternative methodology to carry out the isostatic studies without using directly measured gravity values. We compare the real geoid undulations with the geoid undulations produced by a theoretical balanced model. The actual geoid undulations are extracted from a global geopotential model (EGM96 model) and the theoretical balanced model is constructed using a digital elevation model (GLOBE) from which Airy's roots are assumed (Heiskanen & Moritz 1967). Both data sources are freely-available, avoiding the necessity of field measurement. To perform further analyses the gravity anomalies are derived from the same global geopotential model EGM96 and compared with the gravity anomalies predicted by the same theoretical balanced model. Measured gravity anomalies are also employed for validation.

In order to test the new method, it is applied to the Bolivian Andes, which have been widely studied by different authors employing traditional gravimetry, and show a clear tendency to isostatic balance in Airy hypothesis (Lyon-Caen et al. 1985; Isacks 1988; Abriata & Introcaso 1990; Watts et al. 1995; Götze & Kirchner 1997; Lamb 2000; Introcaso et al. 2000a; Miranda & Introcaso 2000a; Götze & Krause 2002). Present study is preceded by two recent papers in which the geoid undulations along profiles were studied. Introcaso & Introcaso (2004) carried out a crustal analysis from geoid undulations along a profile in the Bolivian Andes at 22ºS, and Miranda & Introcaso (2000b) analyzed geoid values along an East-West section in the Bolivian Andes at 20ºS.

In spite of its application to Bolivian Andes, the methodology here presented is not restricted to high topographies. The authors and collaborators have also tested this methodology for the study of sedimentary basins (e.g., the Salado Basin, see Crovetto et al. 2007), with very promissory results.

METHODOLOGY

The traditional isostatic analysis involves the use of isostatic gravity anomalies. Following the notation of Heiskanen and Moritz (1967), isostatic anomalies are:

$$\Delta g_I = g_0 + F - A_B + A_t + A_C - \gamma \qquad \textbf{(Eq. 1)}$$

where g_0 is measured gravity, F is free-air correction, A_B is Bouguer correction, A_t is terrain correction, A_C is isostatic correction (which depends on the system considered), and γ is normal gravity in the comparison system (for example WGS84 ellipsoid). We need to know g_0 to calculate g_I; that is to say, we need gravimeters to indirectly obtain isostatic anomalies.

The gravity field can be defined in outer space using gravity vectors as well as equipotential surfaces, as the geoid or Earth's physical surface. Geoid can be calculated from: i) gravity anomalies using Stokes' formula or equivalent sources, ii) astrogeodetic deflections of the vertical or differences between ellipsoidal and orthometric heights *h-H*, iii) satellite orbits' deformations, gravity anomalies, deflections of the vertical and general data combination. Geoid undulations computed by technique ii), especially *h-H*, avoid the use of gravimeters. Through technique iii), global geopotential models are constructed.

We will use as input data a digital elevation model and geoid undulations. We will show that it is possible to analyse the isostatic state of a geological structure using these data.

From the digital elevation model can be constructed an isostatically balanced model. The free-air anomaly g_F for such model is:

$$\Delta g_F = g_t + g_c \qquad \textbf{(Eq. 2)}$$

where g_t represents the attraction of the topography (visible masses) and g_c is the attraction of the compensation root (hidden masses). g_c is negative because of the density contrast.

From Eq. 2, the Bouguer anomaly is:

$$\Delta g_B = g_c \qquad \textbf{(Eq. 3)}$$

We can also calculate the theoretical geoid undulations generated by our balanced model, through the computation of the gravity potentials produced by the topographic and the compensation masses. Applying the expression of Bruns (1878), $N = T/\gamma$, geoid undulations N are:

$$N = \frac{1}{\gamma}\left(T_t + T_c\right) \qquad \textbf{(Eq. 4)}$$

where γ is normal gravity (980 mGal), T_t is the topographic perturbing potential and T_c is the compensation root perturbing potential. We adopt the anomalies given by Eq. 2 and Eq. 3, and geoid undulations from Eq. 4 derived from this perfectly balanced model as comparison values.

On the other hand the free-air and Bouguer anomalies can be derived from the actual geoid undulations N' (real expression of the studied zone). Different methods can be applied to obtain the free-air anomaly g'_F (for example: the planar formula of Stokes, equivalent sources or numerical vertical derivation).

From the free-air anomaly g'_F and the digital elevation model, we can compute the Bouguer anomaly g'_B:

$$\Delta g'_B = \Delta g'_F - A_B \qquad \textbf{(Eq. 5)}$$

where $A_B = 2\ G\rho H$ (ρ is the classical correction of Bouguer (ρ_t is the topographic density, G is the gravitational constant and H is the altitude). Comparing g'_F and g'_B anomalies and the "real" geoid undulations N' with those derived from our balanced model [g_F (Eq. 2), g_B (Eq. 3), N (Eq. 4)], the isostatic state and the crustal thickness of the studied area can be evaluated.

This methodology is applied to the study of the Bolivian Andes in the present paper. In the following, several planar approximations are used without taking into account the curvature of the Earth. In addition, the data used (digital elevation model, global geopotential model

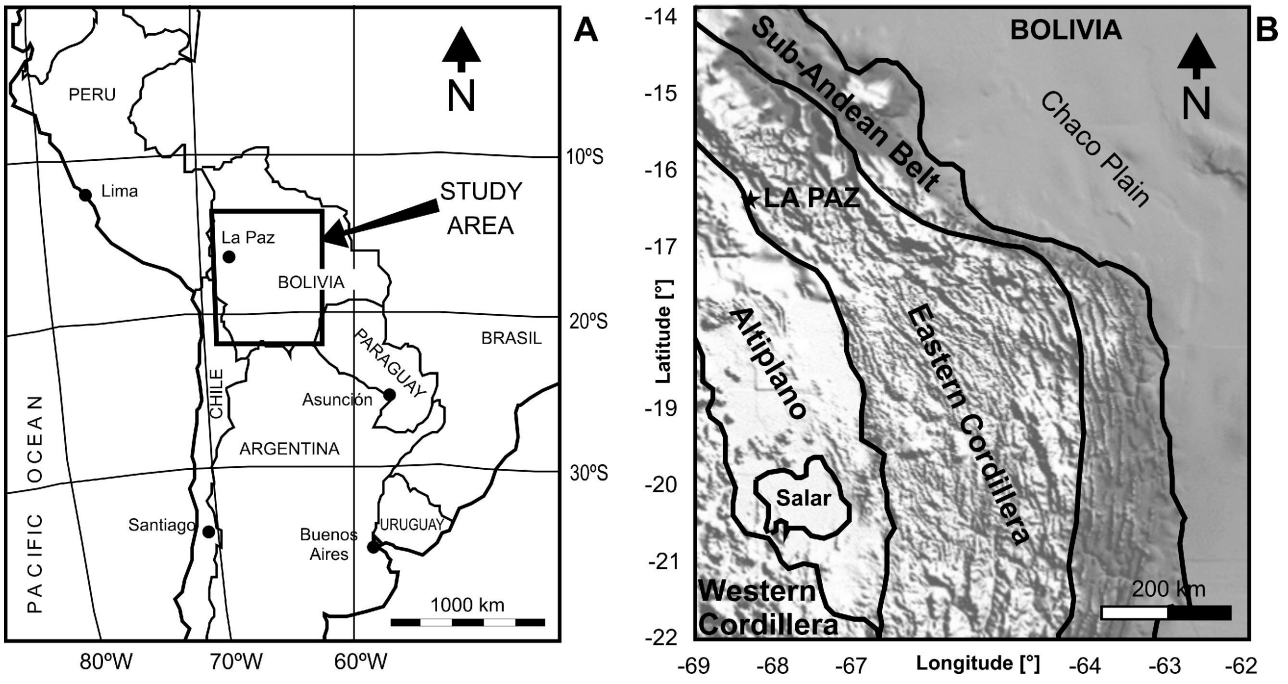

Figure 1. A: Location of the studied area in Bolivia. **B:** Tectonomorphic units of the Andean chain.

for Bolivia and gravity charts) could be not enough accurate to allow the construction of reliable charts. Nevertheless, we consider that the obtained results permit to carry out the regional isostatic analysis within an acceptable accuracy.

STUDY AREA

The study area is located in Bolivia and extends between 14º and 22º South latitude, and 69º and 62º West longitude (Fig. 1A). It comprises the Andean orogen and part of the Chaco Plain (Fig. 1B). The Central Bolivian Andes reach altitudes of 6000 m; the deformation zone extends from the Pacific trench axis to approximately 1000 km into the continent. The Bolivian Andes are divided into parallel tectonomorphic units (Fig. 1B); from west to east: 1) the Western Cordillera is the actual volcanic arc with mountains which locally reach 6000 m altitude; 2) the Altiplano is a high plateau with 3800 m average elevation; 3) the Eastern Cordillera, with mountains reaching 5000 m; 4) the Sub-Andean belt, with mean altitudes of 1500 m and 5) the Chaco Plain. A more detailed description of the tectonomorphic units can be found in Kennan et al. (1995).

Previous geophysical studies (Lyon-Caen et al. 1985; Abriata & Introcaso 1990; Watts et al. 1995; Götze & Kirchner 1997; Miranda & Introcaso 2000a; Götze & Krause 2002) reveal that the Western Cordillera, the Altiplano and the Eastern Cordillera are in isostatic balance considering Airy system, while the Sub-Andes and the Chaco Plain respond to a flexural system. This fact has been interpreted as the result of the flexure of the Brazilian Shield under the load of the Sub-Andes and part of the Eastern Cordillera (Lyon-Caen et al. 1985; Watts et al. 1995; Tassara 2005). Since the aim of the present study is to evaluate the use of geoid undulations to make isostatic studies but not to make a detailed model of the study area, we have considered local equilibrium for the whole area to simplify the theoretical model and to test the proposed methodology.

THEORETICAL ISOSTATIC MODEL

As indicated above the digital elevation model GLOBE (GLOBE Task Team 1999) is used as input signal. Topographic contours for the study area are shown in Fig. 2A. GLOBE is an internationally developed and independently peer-reviewed global digital elevation model (DEM) with 30 arc-seconds latitude-longitude grid spacing. Horizontal precision is in general less than 1 km and vertical precision for South America has a mean square error of 152 m (Hastings & Dunbar 1999). Considering an average elevation of about 3-3.5 km for the studied area, this precision leads to mean altitude errors of about 4-5%. The uncertainty in the computation of the geoid undulations introduced by this error can be easily estimated by employing the one-dimensional approximation from Turcotte & Schubert (1982) as developed below. The uncertainty of 152 m in the topography of an isostatically balanced structure of 3 km mean elevation, introduces an uncertainty of 1 m in the geoid undulations produced by such structure. Considering that the approximation developed by Turcotte & Schubert (1982) over-estimates the geoid undulations in about 10-20% for structures like the one studied here (Crovetto et al. 2006), the average error in the geoid undulations introduced by the error in the digital elevation model is about 0.8-0.9 m, which represents less than 10% of the total undulation, and is considered appropriate for a regional isostatic study.

We assume perfect Airy isostatic balance (Airy 1855) and consider a topographic density $\rho_t = 2.67$ g cm^{-3}, a normal crustal thickness $T_N = 33$ km, and a density

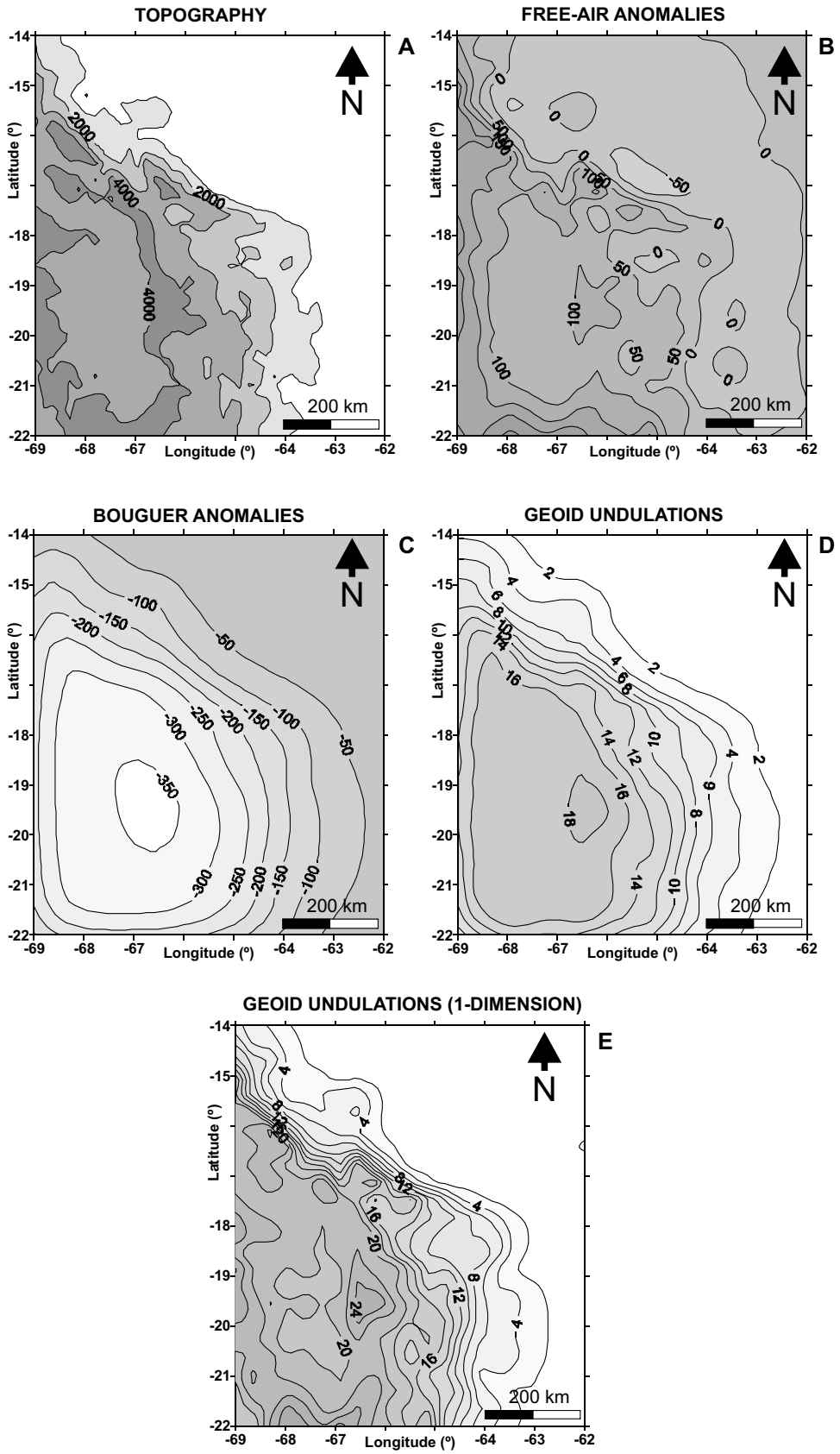

Figure 2. A: Topographic contours for Bolivia from GLOBE digital elevation model (contour interval 1000 m). **B:** free-air anomalies (g_F, contour interval 50 mGal). **C:** Bouguer anomalies (g_B, contour interval 50 mGal). **D:** geoid undulations (*N*, contour interval 2 m) calculated from our isostatic balanced model. **E:** One-dimensional geoid undulations computed from topography using the planar expression from Turcotte & Schubert (1982) (*N*, contour interval 2 m).

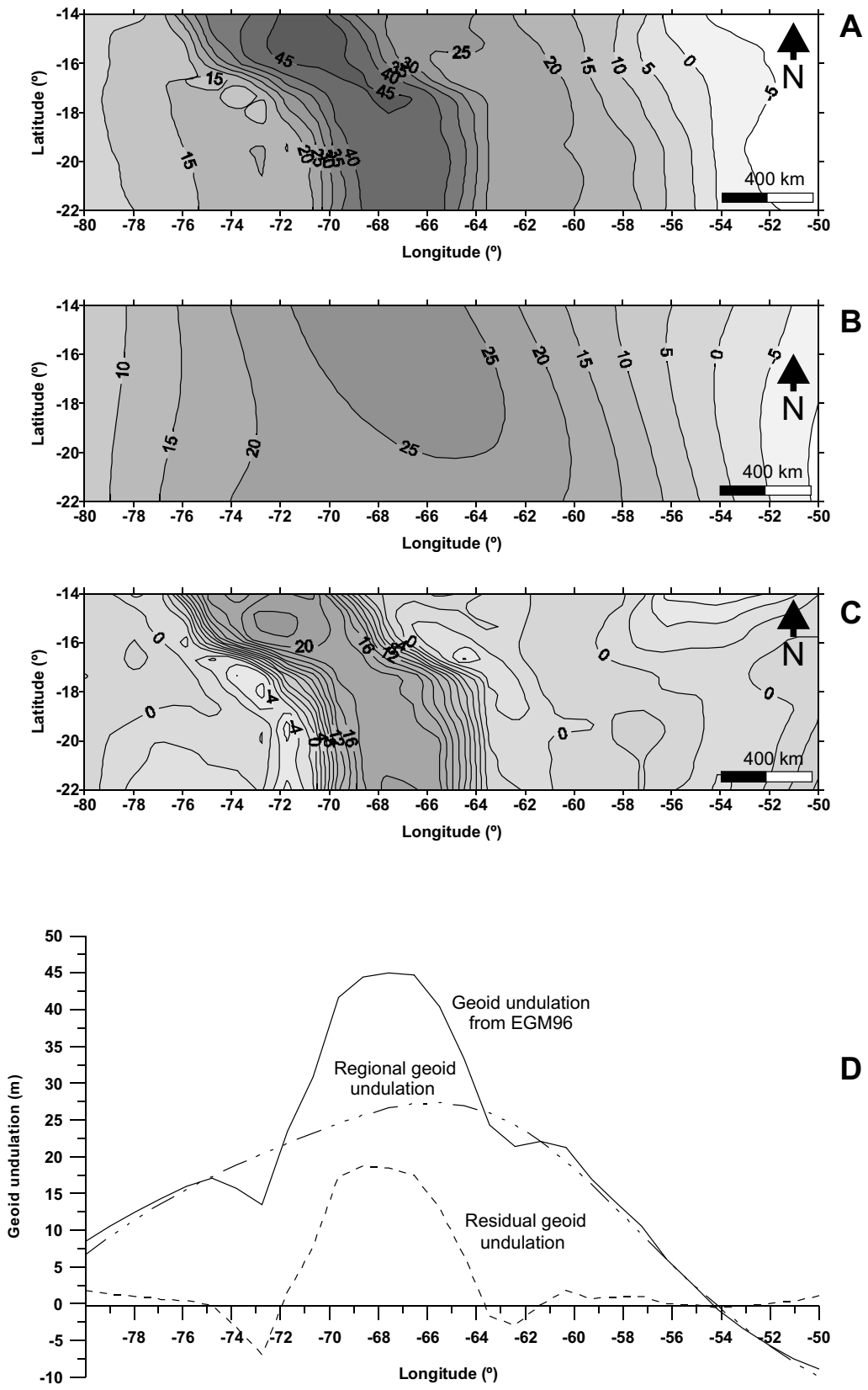

Figure 3. A: Geoid undulations derived from EGM96 geopotential model (contour interval 5 m). **B:** Regional geoid undulations obtained applying the sparse Fourier transform method to the undulations shown in Figure 3A (contour interval 5 m). **C:** Residual geoid undulations (contour interval 2 m). **D:** Profile along 18º S showing EGM96 (solid line), regional (dash and dot line) and residual (dashed line) geoid undulations.

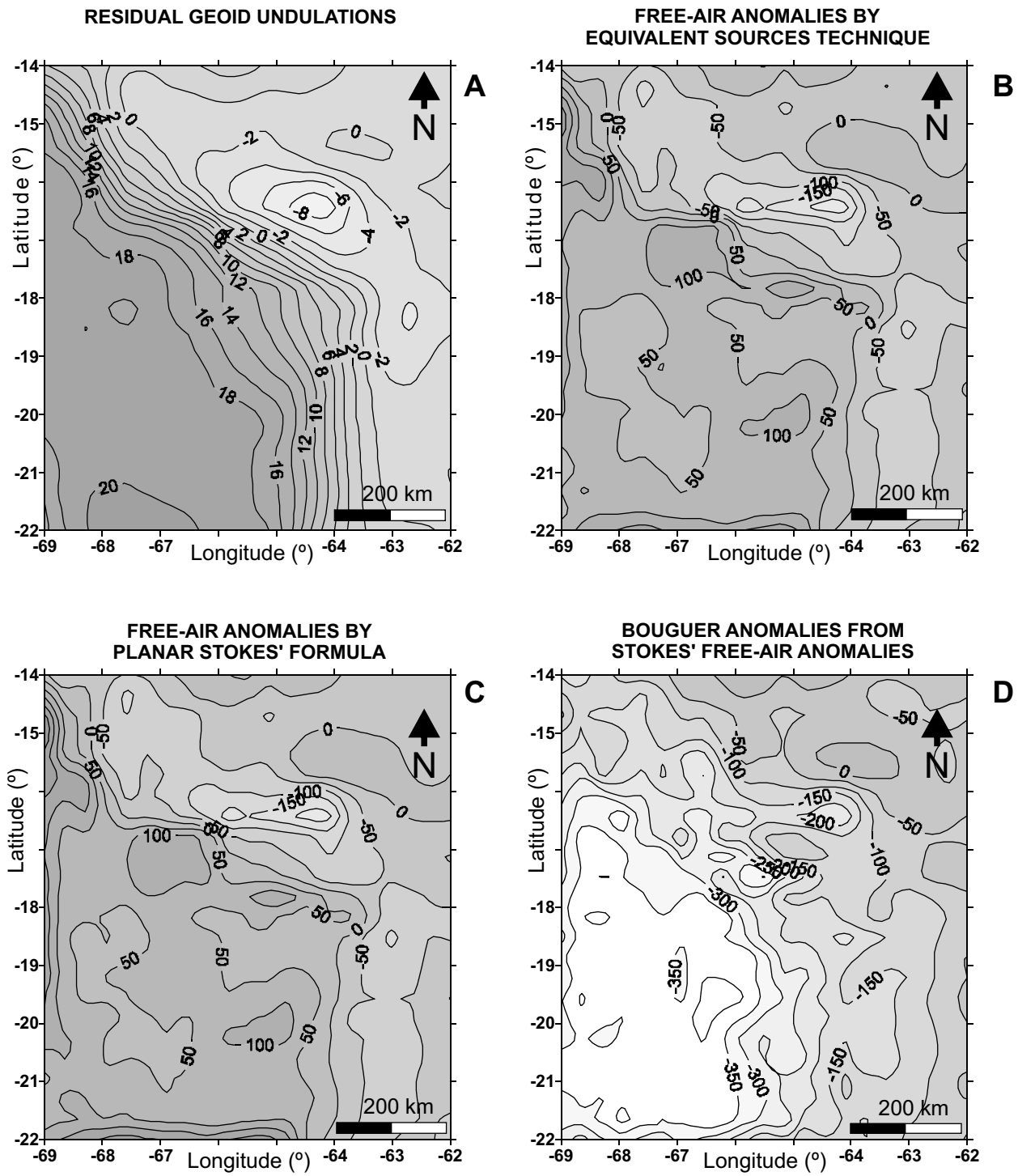

Figure 4. A: Residual geoid undulations for the studied area obtained through the sparse Fourier transform method (contour interval 2 m). **B:** Free-air anomalies obtained from the residual geoid undulations shown in Figure 4A using the equivalent sources technique (contour interval 50 mGal). **C:** Free-air anomalies obtained from the residual geoid undulations shown in Figure 4A with the planar formula of Stokes (contour interval 50 mGal). **D:** Bouguer anomalies derived from the free-air anomalies shown in Figure 4C, using the classical correction of Bouguer and considering the digital elevation model GLOBE (contour interval 50 mGal).

contrast between the lower crust and the upper mantle = -0.4 g cm^{-3} (Introcaso et al. 2000b). Although the study area is large, planar approximations are used. Dipoles contribution to gravity and geoid undulations, produced by a balanced model, decay faster with distance than single-masses contribution because of the compensation between positive and negative masses. Using a simple model, we estimated that the geoid undulations produced by a massive dipole are negligible beyond 150 km. Within such area, differences between spherical formulae and planar approximations are smaller than 4% for close contributions (< 100 km), and smaller than 9% for distant

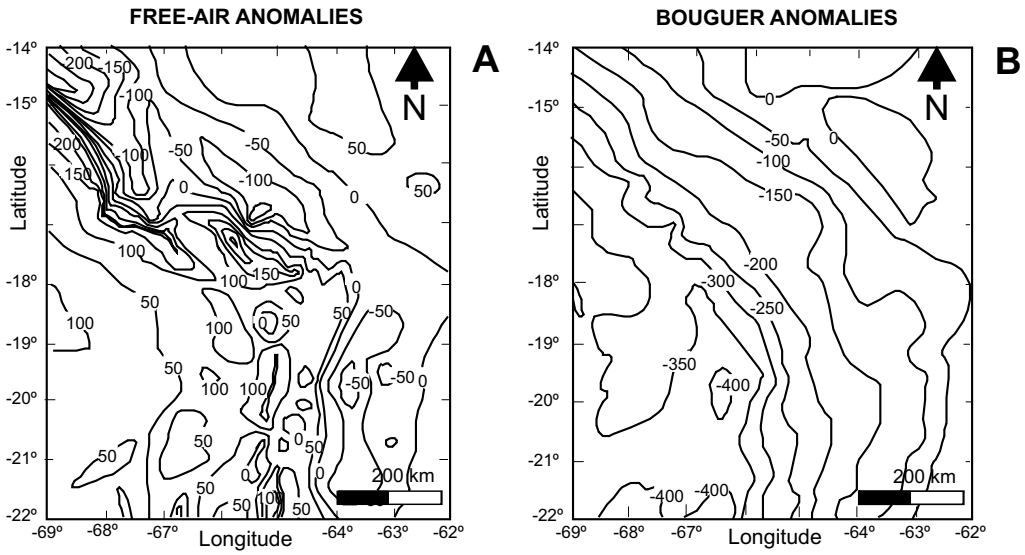

Figure 5. A: Observed free-air anomalies (contour interval 50 mGal). **B:** Observed Bouguer anomalies (contour interval 50 mGal). Source: Military Geographic Institute of Bolivia.

ones (< 150 km). Gravity attractions g_z (x,y,z) of topographic masses and buried compensation masses were computed dividing the corresponding structures in right parallelepipeds. The vertical attraction of a single parallelepiped can be analytically integrated (Introcaso & Huerta 1976; Nagy, 1966) as:

$$g_z(x,y,z) =$$

$$G.\rho \left\| x\ln(y+r) + y\ln(x+r) + 2z\arctan\frac{x+y+r}{z} \right|_{\Delta x_1}^{\Delta x_2} \Big|_{\Delta y_1}^{\Delta y_2} \Big|_{\Delta z_1}^{\Delta z_2}$$

(Eq. 6)

where is the density of the parallelepiped, (x, y, z) are the coordinates of the computation point, x_1, x_2, y_1, y_2, z_1, z_2 are the coordinates of the vertices of the parallelepiped and $r = [(x_i)^2 + (y_i)^2 + (z_i)^2]^{1/2}$ is the distance between the computation point and the parallelepiped vertices with $x_i = x - x_i$, $y_i = y - y_i$, $z_i = z - z_i$, $i = 1, 2$.

Free-air anomalies were calculated adding the attractions of the topographic and compensation masses with their signs using Eq. 2, while buried (i.e. compensation) masses' attractions (placed below the geoid height) were directly interpreted as Bouguer anomalies (Eq. 3). Topographic and compensation masses' gravity potentials $T(x,y,z)$ were also computed dividing the corresponding structures in right parallelepipeds. Using the same notation as in Eq. 6, the potential of a single parallelepiped becomes (Guspí 1999):

$$T(x,y,z) =$$

$$G.\rho \left\| xy\ln(z+r) + xz\ln(y+r) + yz\ln(x+r) + x^2\arctan\frac{y+z+r}{x} + \right.$$

$$\left. + y^2\arctan\frac{x+z+r}{y} + z^2\arctan\frac{x+y+r}{z} \right|_{\Delta x_1}^{\Delta x_2} \Big|_{\Delta y_1}^{\Delta y_2} \Big|_{\Delta z_1}^{\Delta z_2}$$

(Eq. 7)

From the anomalous total potential T generated by the topographic and compensation structures, geoid undulations were calculated using the expression $N = T/$ (Bruns 1878).

Fig. 2A shows the topography (input data) while Fig. 2B-D show the gravity anomalies and the geoid undulations computed for our predictive isostatically balanced model. There is good correlation between the topography and the free-air anomalies, the Bouguer anomalies and the geoid undulations.

In order to evaluate the accuracy of the geoid undulations obtained (Fig. 2D), we also derived them from the digital elevation model, applying the one-dimensional planar formula proposed by Turcotte & Schubert (1982) for continental zones. This expression involves only the topography as input signal, obtaining the geoid undulations through an approximation similar to the slab concept of Bouguer. The geoid undulation produced by an isostatically balanced topography considering this one-dimensional approximation is:

$$N = \frac{\pi G}{\gamma}\rho_{uc}\left[2T_N H + \frac{\rho_{um} + \rho_{uc} - \rho_{lc}}{\rho_{um} - \rho_{lc}}H^2\right] \qquad \textbf{(Eq. 8)}$$

where $_{uc}$ is upper crust density, $_{lc}$ is lower crust density, $_{um}$ is upper mantle density, T_N is normal crustal thickness, and H is orthometric height.

The geoid undulations computed using Eq. 8 (Fig. 2E) are in average 10% higher than those calculated previously (Fig. 2D). Such difference can be attributed to the over-estimation of the structure's mass because of its replacement by an infinite slab, and it is consistent with predicted differences found for one-dimensional approximations (Crovetto et al. 2006). The geoid undulations so obtained validate the geoid undulations obtained by the parallelepiped technique, and show the limitations of these widely employed one-dimensional approximations (Crovetto et al. 2006).

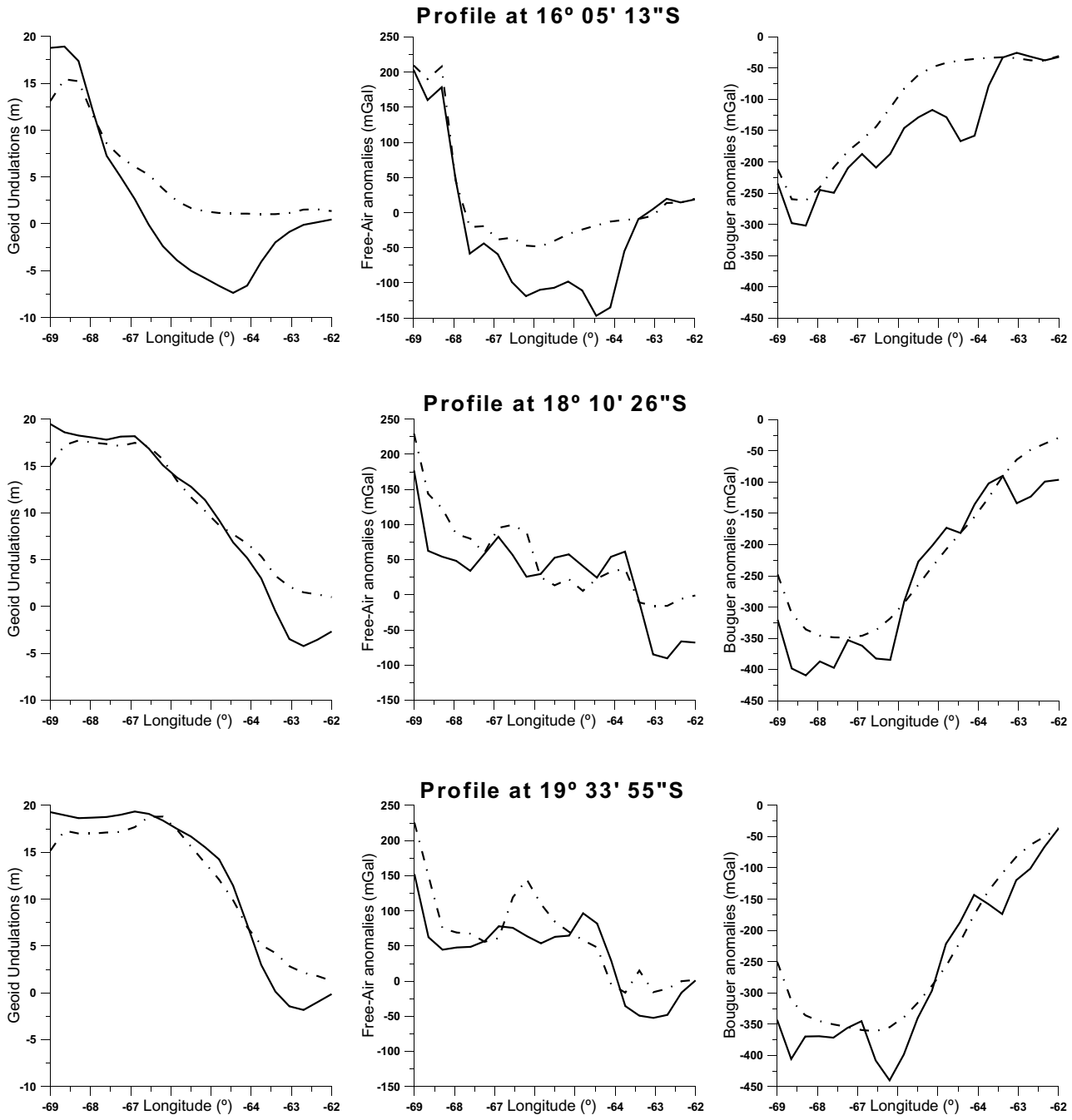

Figure 6. Geoid undulations, free-air and Bouguer anomalies showing observed real values (solid line) and theoretical values (dash and dot line) along profiles at 16º, 18º and 19.5º S approximately.

"REAL" GEOID UNDULATIONS

"Real" geoid undulations were derived from the global geopotential model EGM96 (Lemoine et al. 1998). The poor resolution of this model, with errors of ±1 m in continents (Sideris 1996), introduces an error smaller than 10% in the geoid undulations within our study area. This error, which is compatible with the error of the digital elevation model, is acceptable for a regional isostatic study, and thus we considered the EGM96 model as appropriated for this study.

EGM96 geoid model considers the whole planet masses, involving different wavelengths which must be separated to identify the local effect of the orogen studied here. For discriminating the different components and isolating the Andean effect, EGM96 geoid undulations were calculated for a broader zone including the studied area. The geoid anomaly caused by the Andes can be clearly identified (Fig. 3A). The existence of such anomaly has already been pointed out by Froideveaux & Isacks (1984) and by Introcaso et al. (2000a). For filtering geoid undulations we applied a sparse Fourier transform method (Guspí & Introcaso 2000), which is based on the estimation of a high resolution discrete Fourier transform (DFT). The

incorporation of a priori information allows obtaining a sparse estimate of the DFT, thus the potential field can be defined through a combination of few simple functions. At the same time, low and high frequency components are easily distinguished, allowing us to isolate low frequencies and obtain long wavelengths, which correspond to the regional geoid (Fig. 3B).

The residual geoid undulations (Fig. 3C) were obtained by removing the regional undulations (Fig. 3B) from EGM96 (Fig. 3A). Fig. 3D shows the corresponding total, regional and residual geoid undulations in a profile along 18°S. There is an important similitude between our Fig. 3D and the fig. 3 in Froideveaux & Isacks (1984), where geoid undulations along a section at 20ºS were studied. Fig. 4A shows a more detailed residual geoid undulations map for the studied area.

GRAVITY ANOMALIES FROM RESIDUAL GEOID UNDULATIONS

Using the residual "real" geoid undulations obtained above as input data (Fig. 4A), two different methods were applied to compute the "real" free-air anomaly (Introcaso et al. 2007). In a first approach, the equivalent sources technique was used (Cordell 1992; Guspí et al. 2004). Once the anomalous potential was derived from the residual geoid undulations through the expression of Bruns (1878), a set of punctual masses is obtained, which reproduces the potential field. Then, the gravity attraction corresponding to such masses is computed, and directly interpreted as free-air anomalies (Fig. 4B). In a second approach it was applied the planar formula of Stokes (1849). For obtaining the geoid undulations corresponding to a plain surface, the integral of Stokes (1849) yields:

$$N(x,y) = \frac{1}{2\pi\gamma}\int_{-\infty}^{\infty}\int_{-\infty}^{\infty}\Delta g_F(x',y',0)\left[(x-x')^2+(y-y')^2\right]^{-1/2}dx'dy' \qquad \textbf{(Eq. 9)}$$

where *N(x,y)* represents the undulation at any point *P(x,y)* and $g_F(x'y',0)$ is the free-air anomaly at other point on the geoid. If we assume Helmert condensation method (Heiskanen & Moritz 1967), the indirect effect produced by a topography with a height of 3 km can be easily estimated (Rapp & Wichiencharoen 1984) yielding 0.52 m, while its direct effect on gravity anomalies is 3 mGal. This change from co-geoid to geoid is negligible for our purposes (it represents less than 5 % of total undulation), so we have not considered further corrections. Eq. 9 can be solved dividing the integration surface in rectangular cells, and considering constant gravity within each cell (Introcaso & Crovetto 2005):

$$N(x,y) = \frac{1}{2\pi\gamma}\sum_i\sum_j \Delta g_F(x_i,y_j,0)\cdot F^{ij}(x,y) \qquad \textbf{(Eq. 10)}$$

The function $F^{ij}(x,y) = \iint_{ij-cell}\left[(x-x')^2+(y-y')^2\right]^{-1/2}dx'dy'$ can be integrated analytically (Chapman 1979) and is proportional to the gravity potential produced by the *ij*-cell at the point *P*(*x*,*y*); $g_F(x_i y_j,0)$ is the free-air anomaly at the central point of the *ij*-cell. Considering Eq. 10 as a linear system of equations, free-air anomalies can be obtained from geoid undulations. This free-air anomalies chart (Fig. 4C) show very good correlation with that obtained previously (equivalent sources technique, Fig. 4B), validating our results. From the free-air anomalies (Fig. 4C), the Bouguer anomalies (Fig. 4D) were calculated using the classical correction of Bouguer (Eq. 5), considering a topographic density $_t$ = 2.67 g cm^{-3} and the digital elevation model GLOBE.

MEASURED GRAVITY ANOMALIES

Free-air and Bouguer anomalies charts (Fig. 5), constructed by the Military Geographic Institute of Bolivia in cooperation with the Geophysical Institute of Bolivia (Instituto Geográfico Militar Boliviano 1971, 1972) were also employed. Although these charts are not up to date, they were used for validating the anomalies derived from the global geopotential model EGM96.

DISCUSSION

For the analysis of the isostatic behaviour of the Bolivian Andes, theoretical and "real" geoid undulations and anomalies were compared.

We computed the geoid undulations corresponding to a perfectly balanced isostatic model considering the system of Airy. To calculate such undulations, we used two different techniques: the decomposition of the structure in right parallelepipeds (Fig. 2D) and the planar expression from Turcotte & Schubert (1982), see Fig. 2E. The expression of Turcotte & Schubert (1982) is just an approximation to the real undulations caused by balanced structures, and over-estimates geoid undulations values. The parallelepiped technique is more accurate and also involves *x* and *y* dimensions. In the following analyses, we considered the results obtained applying this last technique.

The residual "real" geoid undulations (Fig. 4A) show qualitative and quantitative correlation with the theoretical geoid undulations (Fig. 2D). The determination coefficient (Hildebrand & Lyman 1997) between "real" and theoretical undulations is 0.76. The main difference between both maps is a negative undulations' zone in the "real" geoid undulations (Fig. 4A), which does not exist in the theoretical ones (Fig. 2D). This zone, located at 16ºS, 64ºW, would correspond to an anomalous zone having no relation with the topography. If we do not consider this anomalous area, the determination's coefficient rises to 0.77. We can also compare "real" and theoretical geoid undulations along the profiles shown in Fig. 6. Along the first profile (16º 05' 13" S), there is poor correlation. This fact could be explained considering that this profile crosses the above mentioned anomalous area. Along the two other profiles (18º 10' 26"S and 19º 33' 55"S) there is very good correlation. The comparison between "real" and theoretical geoid undulations suggests that the Bolivian Andes would show a tendency to isostatic balance in Airy system.

"Real" (Fig. 2B) and theoretical (Fig. 4B and Fig. 4C) free-air anomalies maps show poor correlation. A large area with anomalous values (50-100 mGal) and a well-defined line of 0 mGal crossing the zone from NW to

SE can be seen in both maps. Again, there is an anomalous zone with negative free-air anomalies located at 16ºS, 64ºW. Within that zone, "real" negative anomalies are higher in absolute values (-200 mGal) than those predicted by the theoretical model (-50 mGal), a behaviour uncorrelated with topography. The determination coefficient between the "real" and theoretical free-air anomalies is 0.6 (without considering the anomalous area), indicating poor correlation. The comparison along the profiles in Fig. 6 confirms this behaviour, with a very poor correlation between "real" and theoretical free-air anomalies in the first profile (that which crosses the anomalous area), and a moderate correlation in the other two profiles. This poor correlation between "real" and theoretical free-air anomalies may be attributed to the important oscillation of these anomalies, due to the significant influence of topography (Fig. 2A). This oscillation is not present in Bouguer anomalies, which are more regular (Woollard 1969). The Bouguer anomalies corresponding to the balanced model (Fig. 2C) agree with those derived from EGM96 model (Fig. 4D); both of them show maximum amplitudes of -350 mGal and similar morphology. The "real" Bouguer anomalies present a local minimum (-200 mGal) in the mentioned anomalous area of negative free-air anomalies and geoid undulations located at 16ºS, 64ºW. The determination coefficient between the "real" and the theoretical Bouguer anomalies is 0.84, considering the anomalous area. The comparison between "real" and theoretical Bouguer anomalies along the profiles in Fig. 6 confirms the good correlation.

The anomalous behaviour of "real" free-air and Bouguer anomalies and geoid undulations within the area placed at 16ºS, 64ºW, would suggest that some local isostatic unbalance could exist. The anomalous values found (negative free-air anomalies, negative geoid undulations and negative Bouguer anomalies) deserve further local studies.

Finally we observe that the measured gravity anomalies obtained by the Military Geographic Institute of Bolivia (Fig. 5) are similar to the "real" anomalies derived from the global geopotential model EGM96 (Fig.s 4C-D). This similitude supports the filtering procedure applied to geoid undulations and the methods applied to the computation of gravity anomalies from geoid undulations.

CONCLUSIONS

Crustal and isostatic studies are usually carried out through the comparison of observed gravity anomalies (calculated from gravity values determined by means of gravimeters) with those derived from theoretical isostatically balanced models. Thus, measured gravity values are indispensable for conducting these studies.

Different global geopotential models exist today, which are constructed combining satellite and terrain data. For example, the EGM96 model employed here (Lemoine et al. 1998), and some recently appeared models like the EIGEN-CG01C (Reigber et al. 2004) and the EIGEN-CG03C (Förste et al. 2005). In this work we have shown that comparing the geoid undulations from these global geopotential models with the geoid undulations computed for a perfectly isostatically balanced model, it is possible to carry out isostatic studies without the use of measured gravity values. The results of such comparison could be validated by employing for example *h-H* geoid undulations values, which are independent of the global geopotential models. From these global geopotential models, it is also possible to derive the free-air and Bouguer gravity anomalies. The comparison between such anomalies and those calculated for the perfectly isostatically balanced model allows an alternative comparison to be done.

The new methodology proposed in this paper was employed to make an isostatic analysis of Bolivia as case study. Results suggests that Bolivian Andes are in local isostatic balance (Airy 1855), with the exception of an anomalous zone located at 16ºS, 64ºW in the Chaco Plain. These results are in very good agreement with previous studies conducted with traditional gravimetry for that area (Lyon-Caen et al. 1985; Isacks 1988; Abriata & Introcaso 1990; Watts et al. 1995; Götze & Kirchner 1997; Miranda & Introcaso 2000a; Götze & Krause 2002), showing the good performance of the new methodology.

Acknowledgements.- Carolina Crovetto would like to acknowledge Fundación Josefina Prats and CONICET for their economical support in her PhD studies. This work was partially supported by ANPCYT PICTR 2002-00166. Alberto H. Comínguez and two further anonymous reviewers of the journal contributed for enhacing the manuscript of this paper.

REFERENCES

Abriata J.C. & Introcaso, A., 1990. Contribución gravimétrica al estudio de la transecta ubicada al sur de Bolivia. *Revista del Instituto Geográfico Militar, Año 5,* **7**: 8-19.

Airy G.B., 1855. On the computation of the effect of the attraction of mountain-masses, as disturbing the apparent astronomical latitude of stations of geodetic surveys. *Philosophical Transactions of the Royal Society of London* **145:** 101-104.

Bruns H., 1878. Die Figur der Erde. *Publikation Königl Preuss. Geodetic Institut Stankiewicz Buchdrukerei,* 98 p. Berlin.

Chapman M. E., 1979. Techniques for interpretation of geoid anomalies. *Journal of Geophysical Research* **84 (B8)**: 3793-3801.

Cordell L., 1992. A scattered equivalent-source method for interpolation and gridding of potential-field data in three dimensions. *Geophysics* **57(4)**: 629-636.

Crovetto C., Molinari R. & Introcaso A., 2006. Aproximaciones para el cálculo del geoide isostático. *Revista de la Asociación Geológica Argentina* **61(3)**: 38-48.

Crovetto C.B., Novara I.L. & Introcaso A., 2007. A stretching model to explain the Salado Basin (Argentina). *Boletín del Instituto de Fisiografía y Geología* **77(1-2):** 1-10.

Förste C., Flechtner F., Schmidt R., Meyer U., Stubenvoll R., Barthelmes F., König R., Neumayer K.H., Rothacher M., Reigber Ch., Biancale R., Bruinsma S., Lemoine J.-M. & Raimondo J.C., 2005. A new high resolution global gravity field model derived from combination of GRACE and CHAMP missions and altimetry/gravimetry surface gravity data. *EGU General Assembly 2005, Vienna, Austria*: 24-29. http://www.gfz-potsdam.de/pb1/op/grace/results/index_RESULTS.html.

Froideveaux C. & Isacks B., 1984. The mechanical state of the lithosphere in the Altiplano-Puna segment of the

Andes. *Earth & Planetary Science Letters* **71**: 305-314.

GLOBE Task Team and others (Hastings D., Dunbar P., Elphingstone G., Bootz M., Murakami H., Maruyama H., Masaharu H., Holland P., Payne J., Bryant N., Logan T., Muller J., Schreier G. & MacDonald J.), 1999. The Global Land One-kilometer Base Elevation (GLOBE) Digital Elevation Model, Version 1.0. *National Oceanic and Atmospheric Administration, National Geophysical Data Center, 325 Broadway, Boulder, Colorado 80303, U.S.A*. Digital data base at http://www.ngdc.noaa.gov/mgg/topo/globe.html.

Götze H.-J. & Kirchner A., 1997. Interpretation of gravity and geoid in the Central Andes between 20º and 29ºS. *Journal of South American Earth Sciences* **10(2)**: 179-188.

Götze H.-J. & Krause S., 2002. The Central Andean gravity high, a relic of an old subduction complex?. *Journal of South American Earth Sciences* **14**: 799-811.

Guspí F., 1999. Fórmulas compactas para el cálculo del potencial gravitatorio de prismas rectangulares. En: *Contribuciones a la Geodesia en la Argentina de fines del siglo XX – Homenaje a Oscar Parachú. UNR Editora:* 129-133.

Guspí F. & Introcaso B., 2000. A sparse spectrum technique for gridding and separating potential field anomalies. *Geophysics* **65(4)**: 1154-1161.

Guspí F., Introcaso A. & Introcaso B., 2004. Gravity-enhanced representation of measured geoid undulations using equivalent sources. *Geophysical Journal International* **158**: 1-8.

Hastings D. & Dunbar P., 1999. Global Land One-kilometer Base Elevation (GLOBE) Digital Elevation Model. *Documentation, Volume 1.0. Key to Geophysical Records Documentation (KGRD) 34. National Oceanic and Atmospheric Administration, National Geophysical Data Center, Boulder, Colorado*. http://www.ngdc.noaa.gov/mgg/topo/globe.html.

Heiskanen W. & Moritz H., 1967. Physical Geodesy. *W. Freeman and Company*, 364 pp., San Francisco.

Hildebrand D. & Lyman Ott R., 1997. Estadística aplicada a la administración y a la economía. *Addison Wesley Longman*, 943 pp.

Introcaso A. & Huerta E., 1976. Valuación de efectos gravimétricos y sus aplicaciones a la interpretación. *Geoacta* **8(1)**: 75-98.

Introcaso A., Cornaglia L. & Pacino M.C., 2000a Gravimetría en los segmentos andinos en 23ºS y 35ºS. Acortamientos, estado isostático y modelos corticales. *Actas del 22° Simposio sobre Latinoamérica, Stuttgart, Alemania* **18**: 49.

Introcaso A., Pacino M.C. & Guspí F., 2000. The Andes of Argentina and Chile: Crustal configuration, isostasy, shortening and tectonic features from gravity data. *Temas de Geociencia* **5**: 1-31.

Introcaso A. & Introcaso B., 2004. Estudio cortical en una sección de los Andes Bolivianos a partir de ondulaciones del geoide. *16 Congreso Geológico Boliviano, Oruro, Bolivia, 4 pp.* **[MSD 2]**

Introcaso A. & Crovetto C., 2005. Introducción a la construcción del geoide. *Temas de Geociencia* **12**: 1-56.

Introcaso A., Crovetto C.B., Introcaso B. & Ruiz F., 2007. Construction of gravity charts without observed gravity data. *Bolletino di geodesia e scienze affini* **66(4)**: 189-209.

Instituto Geográfico Militar Boliviano (en cooperación con el Instituto Geofísico Boliviano), 1971. Carta de anomalías de Bouguer de Bolivia. Escala 1:2.500.000.

Instituto Geográfico Militar Boliviano (en cooperación con el Instituto Geofísico Boliviano), 1972. Carta de anomalías de aire libre de Bolivia. Escala 1:2.500.000.

Isacks B., 1988. Uplift of the Central Andes plateau and bending of the Bolivian orocline. *Journal of Geophysical Research* **93**: 3211-3231.

Kennan L., Lamb S. & Rundle C., 1995. K-Ar dates from the Altiplano and Cordillera Oriental of Bolivia: implications for Cenozoic stratigraphy and tectonics. *Journal of South American Earth Sciences* **8(2)**: 163-186.

Lamb S., 2000. Active deformation in the Bolivian Andes, South America. *Journal of Geophysical Research*, **105(B11)**: 25627-25653.

Lemoine F., Kenyon S., Factor J., Trimmer R., Pavlis N., Chiuw D., Cox C., Klosko S., Lutheke S., Torrence M., Wang Y., Williamson R., Pavlis H., Rapp R. & Olson T., 1998. The development of the joint NASA, CSFC and NIMA geopotential model EGM96. *NASA/TP, Technical Report 1998 – 206861, Goddard Space Flight Center,* 575 pp. URL: http://cddis.nasa.gov/926/egm96/egm96.html.

Lyon-Caen H., Molnar P. & Suárez G., 1985. Gravity anomalies and flexure of the Brazilian Shield beneath the Bolivian Andes. *Earth and Planetary Science Letters* **75:** 81-92.

Miranda S. & Introcaso A., 2000a. Acortamientos corticales para los Andes Centrales Bolivianos a partir de datos de gravedad. *Actas del Noveno Congreso Geológico Chileno, Puerto Varas, Chile* **2**: 593-597.

Miranda S. & Introcaso A., 2000b. Anomalías de ondulación del geoide isostático para los Andes Centrales de Bolivia en 20ºS. Actas del *Vigésimo Congreso de la Asociación Argentina de Geofisicos y Geodestas, Mendoza, Argentina*: 207-211. **[MSD 1]**

Nagy D., 1966. The gravitational attraction of a right rectangular prism. *Geophysics* **31(2)**: 362-371.

Pratt J.H., 1855. On the attraction of the Himalaya mountains, and of the elevated regions beyond them, upon the plumb line in India. *Philosophical Transactions of the Royal Society of London* **14:** 53-100.

Rapp R. & Wichiencharoen C., 1984. A Comparison of Satellite Doppler and Gravimetric Geoid Undulations Considering Terrain-Corrected Gravity Data. *Journal of Geophysical Research* **89(B2)**: 1105-1111.

Reigber Ch., Schwintzer P., Stubenvoll R., Schmidt R., Flechtner F., Meyer U., König R., Neumayer H., Förste Ch., Barthelmes F., Zhu S.Y., Balmino G., Biancale R., Lemoine J.-M., Meixner H. & Raimondo J.C., 2004. A High Resolution Global Gravity Field Model Combining CHAMP and GRACE Satellite Mission and Surface Gravity Data: EIGEN-CG01C. URL: http://www.gfz-postdam.de/grace/results/index_results.html

Sideris M.,1996. International tests of the new GSFC/DMA Geopotential Models. Gravity, Geoid and Marine Geodesy. *International Association of Geodesy Symposia (Tokyo)* **117**: 478-485.

Stokes G.G., 1849. On the variation of gravity on the

surface of the earth. *Transactions of the Cambridge Philosophical Society* **8**: 672-695.

Tassara A., 2005. Interaction between the Nazca and South American plates and formation of the Altiplano-Puna plateau: Review of a flexural analysis along the Andes margin (15º-34ºS). *Tectonophysics* **399**: 39-57.

Turcotte D. L. & Schubert, G. 1982. Geodynamics. Applications of continuum physics to geological problems. *John Wiley & Sons Ed., New York*, 450 pp.

Vening Meinesz F.A., 1931. Une nouvelle méthode pour la réduction isostatique régionale de l'intensité de la pesanteur. *Bulletin Géodésique* **29**: 35-51.

Watts A.B., Lamb S.H., Fairhead J.D. & Dewey J.F., 1995. Lithospheric flexure and bending of the Central Andes. *Earth and Planetary Science Letters* **134**: 9-21.

Woollard G., 1969. Regional Variations in Gravity. *Geophysical Monograph, American Geophysical Union* **13**: 320-341.

GEOID UNDULATIONS CHART OF THE SAN LUIS RANGE (ARGENTINA). GEOPHYSICAL APPLICATION

Laura L. CORNAGLIA & Antonio INTROCASO

Boletín del Instituto de Fisiografía y Geología

Cornaglia L.L. & Introcaso A., 2008. Geoid undulations chart of the San Luis range (Argentina). Geophysical application. *Boletín del Instituto de Fisiografía y Geología* **78(1-2)**: 13-22. Rosario, 02-12-2008. ISSN 1666-115X.

Abstract.- In this work we show that it is possible to define the isostatic state of a geological structure using a geoid undulations chart. We have built: (1) a detailed geoid undulations chart of the San Luis range area using (a) the global geopotential model EIGEN CG03C for long wavelength free-air gravity anomalies and geoid undulations, and (b) observed residual free-air gravity anomalies and the equivalent sources method for short wavelength geoid undulations, and (2) a theoretical undulations chart of San Luis range area, involving effects from an isostatically compensated model. By comparing charts (1) and (2) we have found agreement between them, thus indicating the San Luis range is rather well isostatically balanced.

Key-words: Geological structure; Geoid; Isostasy.

Resumen.- ***Carta de ondulaciones del geoide de la Sierra de San Luis (Argentina). Aplicación geofísica.*** Nuestro propósito es demostrar que desde una carta de ondulaciones del geoide de buena resolución es posible inferir las características corticales de una estructura geológica. Para ello construimos: (1) una carta de ondulaciones del geoide sobre la sierra de San Luis con adecuado detalle empleando (a) anomalías de aire libre y ondulaciones del geoide de largas longitudes de onda provenientes del modelo global geopotencial EIGEN CG03C y (b) anomalías de aire libre residuales observadas y el método de fuentes equivalentes para calcular las ondulaciones del geoide de cortas longitudes de onda, y (2) una carta de ondulaciones del geoide que contiene los efectos isostáticos de un modelo perfectamente compensado. Comparando ambas cartas (1) y (2) encontramos una muy aceptable coincidencia entre ambas, indicando un buen balance isostático para la sierra de San Luis.

Palabras clave: Estructura geológica; Geoide; Isostasia.

Laura L.Cornaglia: *Instituto Geofísico Sismológico Volponi (UNSJ), Meglioli 1160 (S), 5400 San Juan, Argentina, Grupo de Geofísica, IFIR (CONICET-UNR), Pellegrini 250, 2000 Rosario, Argentina.*

Antonio Introcaso: *Facultad de Ciencias Exactas, Ingeniería y Agrimensura (UNR), Grupo de Geofísica, IFIR (CONICET-UNR), Pellegrini 250, 2000 Rosario, Argentina.*

Received: 01/08/2008; accepted: 15/11/2008.

INTRODUCTION

The San Luis range is located NE of the homonymous Province, west-central Argentina. The range boundaries are: 32º00'- 33º30' S and 65º00'- 66º30' W. The range extends over 23000 km^2 along an imaginary axis 150 km long and NE strike. The range is 80 km wide. Altitudes are less than 2000 m. Three sedimentary basins are located arround the San Luis range: Las Salinas in the Northwest, Beazley in the South, Mercedes in the Southeast and Conlara Valley apart from the San Luis range of Comechingones range (Fig. 1).

Cornaglia & Introcaso (2004), working on a profile, have preliminarily pointed out a crustal thickness excess in the area; Crovetto & Introcaso (2004) have proposed short wavelength isostatic geoidic indicators to make a preliminary isostatic analysis of the San Luis range, concluding that geoid undulations allow validating classic gravimetry; Introcaso & Crovetto (2005) have presented different methods for building a geoid chart, in particular a chart for the San Luis range. All previous works on the San Luis range have presented preliminary conclusions because of the lack of consistent geoid undulations charts.

In this work we present a high resolution geoid undulations chart built using an equivalent sources method and observed free-air gravity anomalies (Fig. 2), practically Faye anomalies in view of the maturity of the topography. We have first obtained long wavelength geoid undulations (N_{LWL}) using adequate cuts in the spherical harmonic expansions. We have used the global geopotential models EGM96 (Lemoine et al. 1998) and EIGEN GL03C (Förste et al. 2005). Then, from residual free-air gravity anomalies and equivalent sources methods, we have obtained short wavelength geoid undulations N_{SWL}. Total geoid undulations are: $N_T = N_{LWL} + N_{SWL}$. This expression was adjusted in eleven geoid height stations $N = h - H$ (see Fig. 3). Finally, from San Luis range topographic altitudes, we have built an isostatically balanced model defined using T_N (standard crustal thickness): 33 km and R (crustal root bellow T_N) = 6.675 H_T, being H_T the topographic altitude. From direct calculation and using right and homogeneous parallelepipeds we have obtained theoretical residual free-air gravity anomalies corresponding to the isostatically compensated model. Then, using the equivalent sources method, we have obtained the disturbing potential T and the isostatic geoid undulations N_{iSWL}. Total isostatic geoid undulations are $N_{iT} = N_{LWL} + N_{iSWL}$. By comparing N_T and N_{iT} we have found that the San Luis range is isostatically rather well balanced.

BRIEF DESCRIPTION OF THE SAN LUIS RANGE

Jordan & Allmendinger (1986) have pointed out that the Pampeanas Ranges geological province of Argentina is a region of large mountains. It is located on the western side of the thin skinned thrust belt of the Andean Mountains, coincident with a region where the subducted Nazca plate is sub-horizontal. Mountain ranges have been uplifted by reverse faulting and local folding. There are evidences of compressional earthquakes. The nearest shortening is estimated to be about 2%. Many of the faults are listric in the subsurface and flatten at mid to lower crustal depths. In opinion of Sato et al. (2003), the

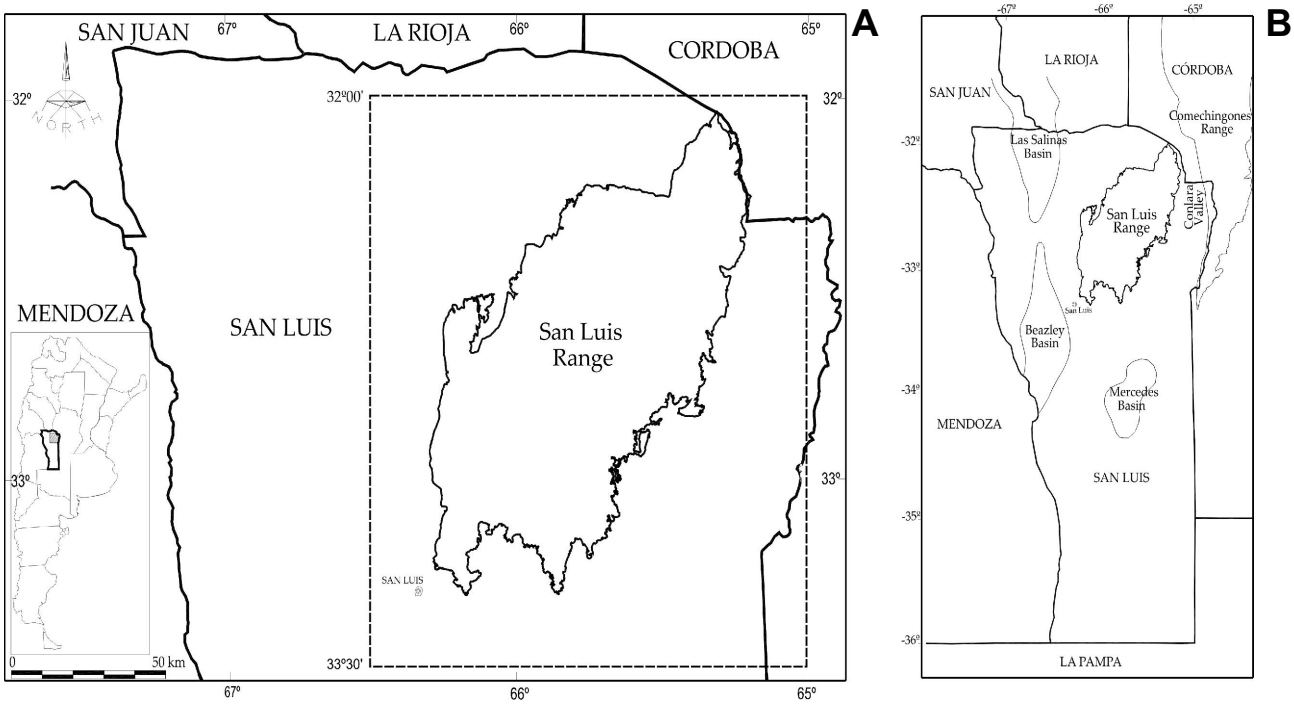

Figure 1. A: Geographic location of the San Luis range. **B**: Location of the sedimentary basins nearby the San Luis range (Modified from Criado-Roqué et al. 1981).

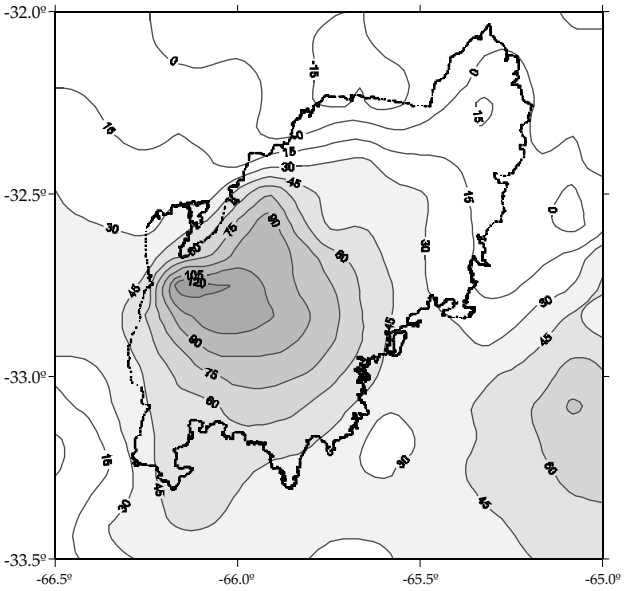

Figure 2. Observed free-air anomalies chart. Equidistance 15 mGal.

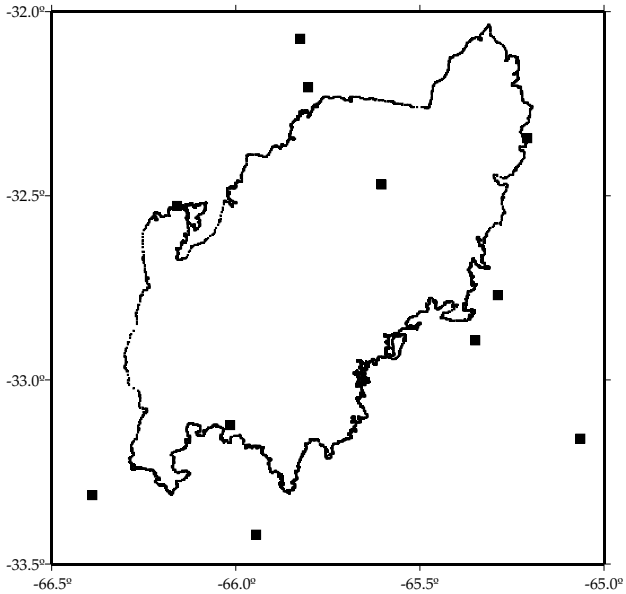

Figure 3. Geographic location of the geoid height stations $N = h - H$ of the San Luis Provincial Geodetic Network. Values $N = h - H$ were used as the control of N_T obtained in this work.

San Luis range basement is igneous-metamorphic. The main phase of the Famatinian orogenic cycle was responsable for delineating the most important features of the San Luis range basement. The Famatinian magmatic arc was active since Mid-Cambrian times (513 – 501 Ma) and the Ordovician was the climax of the magmatism, tectonism and metamorphism. From the regional point of view, the Ordovician deformation in Pampeanas Ranges was associated with terrane collision. The San Luis range is located at the proto-Andean margin on the Gondwana autochthon where the magmatic arc was emplaced.

DATA BASE

In this work we use gravity data and levelling heights. Both of them were obtained from IFIR (Instituto de Física Rosario) and IGM (Instituto Geográfico Militar) data bases. IFIR gravity measurements before 1997 have standard deviations of ± 0.3 mGal (Introcaso et al. 1992); 1997 IGM and IFIR gravity measurements present standard deviations of ± 0.1 mGal (Geophysics Group, IFIR). Values from Argentine Gravity Chart (Guspí et al. 1995) were incorporated to the calculations in order to avoid Gibbs phenomena.

Using the whole gravity values, free-air anomalies were calculated in IGSN 1971 system. On the other hand, long wavelength free-air anomalies obtained from both global geopotential EGM96 (Lemoine et al. 1998) and EIGEN GL03C (Förste et al. 2005) models were used in our calculations. Altimetry used here involves: (a) bench marks heights from IGM, (b) heights obtained from different gravity profiles on the San Luis range from IFIR data base, and (c), heights from digital elevation model (Gtopo30, U.S. Geological Survey EROS Data Center (EDC), 1996). Precision orders of these altitudes are: in (a), $\pm 3\text{mm}(L[\text{km}])^{½}$ and $\pm 5\text{mm}(L[\text{km}])^{½}$ for high precision lines and precision lines respectively; $\pm 10\text{cm}(L[\text{km}])^{½}$ for topographic lines with L: lenght measured line in km; in (b), ±1.00m (Geophysics Group, IFIR) and in (c) by comparing 269 heights on bench marks (high precision line and precision line) and altitudes in the same stations from the digital elevation model, we have obtained a relative porcentual error of 5 % (Cornaglia 2005). If we translate these values to gravity calculations, the maximum error on the observed anomalies is: (a) ±0.03mGal; (b) ±0.30mGal and (c), ±3.06mGal (only fitted values). These probability errors are adequated for our aims. So, different weights were assumed for building regular grids of observed free-air gravity anomalies.

We consider all values used here consistent enough to obtain a geoid undulations N chart to study the isostatic state of the San Luis range according to our purposes.

Gravity anomaly. Observed gravity values g_{Obs} used here were connected to the fundamental Miguelete station of Buenos Aires (Argentina): 979690.03 mGal corresponding to IGSN71 [International Gravity Standarization Network 1971]. Then, we have used the traditional expression:

$$AAL = g_{\text{Obs}} - (\quad - c_{\text{AL}}) \qquad \textbf{(Eq. 1)}$$

where AAL is the free-air gravity anomaly (in mGal) (Fig. 2), is the normal gravity calculated with WGS84 ellipsoid and c_{AL} is the free-air correction, with $c_{\text{AL}} = 0.3086\ H$ [mGal/m], being H: the altitude of the station. These free-air anomalies were assumed as Faye anomalies because, in view of the maturity of the relief, the terrain corrections are less than 4% (Cornaglia 2005). From Eq. 1 is possible to separate both free-air long wavelength and short wavelength anomalies.

Table 1. Amount of stations according to $E = N_T - N_C$ for different truncated spherical harmonic expansions. Proportionality factor k = 1.4 was assumed to define equivalent sources depth. In column (1) $E = N_T - N_C$ intervals assumed, with N_T: total geoid undulations obtained from Eq. 3, N_C: geoid undulations from the geometric definition $N_C = h - H$ (order precision approx. ± 0.05 m, see Figure 3) and E: residual difference; in column (2), the amount of stations for intervals E vs N_{LWL} from the EIGEN CG03C spherical harmonic expansion model truncated at $n = m =$ 36, 40, 50 and 70 respectively, and on third column (3), EGM96 model results. Shaded cells point out that the largest amount of stations for the smallest E interval belongs to EIGEN CG03C model.

	PROPORTIONALITY FACTOR 1.4								
	Degree and order truncation								
(1)	(2)				(3)				
$N_T - N_C = E$ Intervals [m]	EIGEN CG03C				EGM96				
	36	40	50	70	36	40	50	70	
0.00-0.25	5	8	4	5	6	5	4	5	Amount of Stations
0.25-0.50	4	2	5	4	2	5	5	4	
0.50 -0.75	1	1	1	1	2	0	1	1	
0.75 -1.00	1	0	1	1	1	1	1	1	

Table 2. Amount of stations according to $E = N_T - N_C$ for different truncated spherical harmonic expansions. Proportionality factor k = 2.1 was assumed to define equivalent sources depth. Columns (1) - (3) as in Table 1.

	PROPORTIONALITY FACTOR 2.1								
	Degree and order truncation								
(1)	(2)				(3)				
$N_T - N_C = E$ Intervals [m]	EIGEN CG03C				EGM96				
	36	40	50	70	36	40	50	70	
0.00-0.25	5	8	4	5	5	5	5	6	Amount of Stations
0.25-0.50	4	2	5	4	3	5	3	3	
0.50 -0.75	1	1	1	1	2	1	2	1	
0.75 -1.00	1	0	1	1	1	0	1	1	

Table 3. Amount of stations according to $E = N_T - N_C$ for different truncated spherical harmonic expansions. Proportionality factor k = 2.8 was assumed to define equivalent sources depth. Columns (1) - (3) as in Table 1.

	PROPORTIONALITY FACTOR 2.8								
	Degree and order truncation								
(1)	(2)				(3)				
$N_T - N_C = E$ Intervals [m]	EIGEN CG03C				EGM96				
	36	40	50	70	36	40	50	70	
0.00-0.25	6	6	4	6	4	4	5	6	Amount of Stations
0.25-0.50	2	4	5	1	4	5	3	3	
0.50 -0.75	3	1	2	3	2	2	2	1	
0.75 -1.00	0	0	0	1	1	0	1	1	

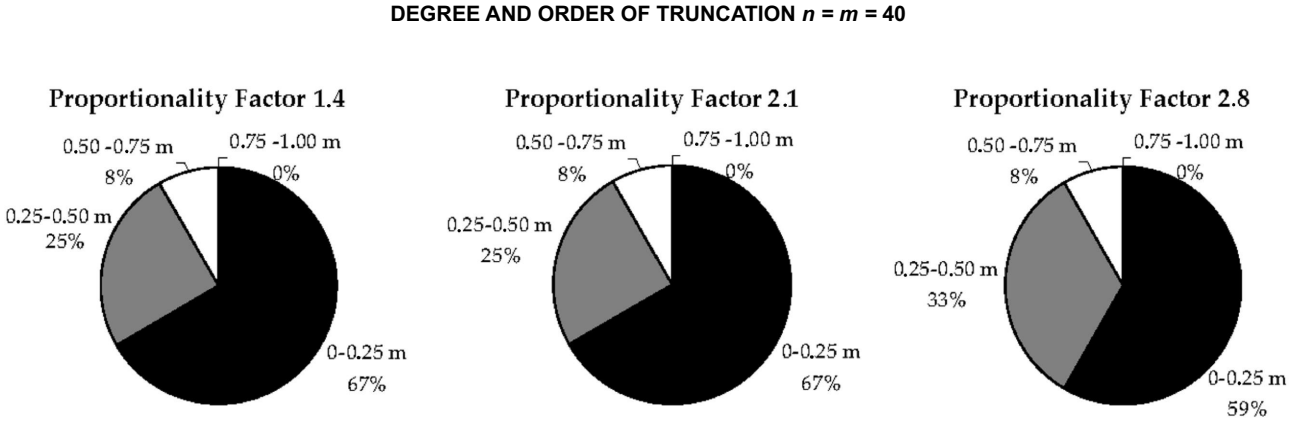

Figure 4. Percentage of amount of stations in order to $E = N_T - N_C$ differences corresponding to $n = m = 40$ EIGEN CG03C in relation to the different proportionality factors used in calculation.

GEOID UNDULATIONS CHART OF THE SAN LUIS RANGE

Although the well known ambigüity of potential field is a serious problem to obtain a consistent gravity model by inversion, it can be put into advantage to calculate geoid undulations (Introcaso 2004, 2006). From the equivalent sources method (fictitious, simple, rigurous), it is possible to define a model (ensemble of sources) that fits observed free-air anomalies removed from long wavelength effects. Then, from this fictitious model, we can directly calculate the disturbing potential (or anomalous potential) T, then obtain N from the formula of Bruns: $N = T/$ (see Torge 2001) with $= 9.80$ m/s^2 (Guspí et al. 2004, Introcaso & Crovetto 2005, Introcaso 2006). We have followed Guspí et al. (2004) who solved a linear equations system:

$$N_i = \frac{1}{\gamma}\sum_{j=1}^{n} T_{ji} = \frac{1}{\gamma}\,\mathrm{G}\sum_{j=1}^{n}\frac{c_{ji}}{l_{ji}} \qquad \textbf{(Eq. 2)}$$

for obtaining the intensities of equivalent sources c_j. G is the gravitational constant $6.67\text{x}10^{-8}$ cm^{3}g^{-1}s^{-2}, T_{ji} is the disturbing potential at i station and l_{ji} is the distance from the station i to the source c_j. In order to calculate different long wavelength geoid undulations, the following expression was assumed:

$$N_T = N_{LWL} + N_{SWL} \qquad \textbf{(Eq. 3)}$$

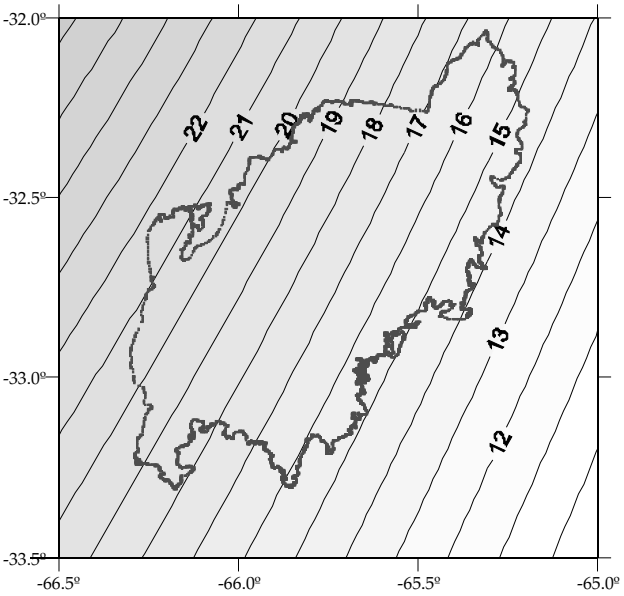

Figure 5. Free-air gravity anomalies AAL_{LWL} chart from EIGEN CG03C model developed up to $n = m = 40$. Contours each 1 mGal.

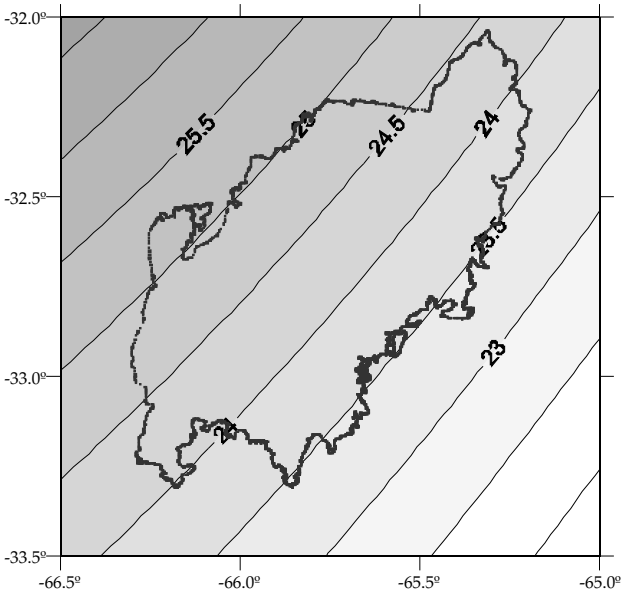

Figure 6. Geoid undulations N_{LWL} chart from EIGEN CG03C model developed up to $n = m = 40$. Contours each 0.25 m.

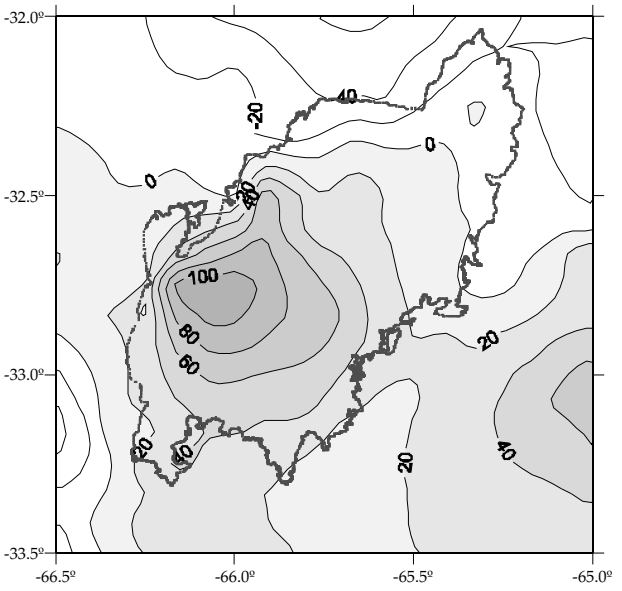

Figure 7. Short wavelength free-air anomalies chart obtained from Eq. 4. Contours each 15 mGal.

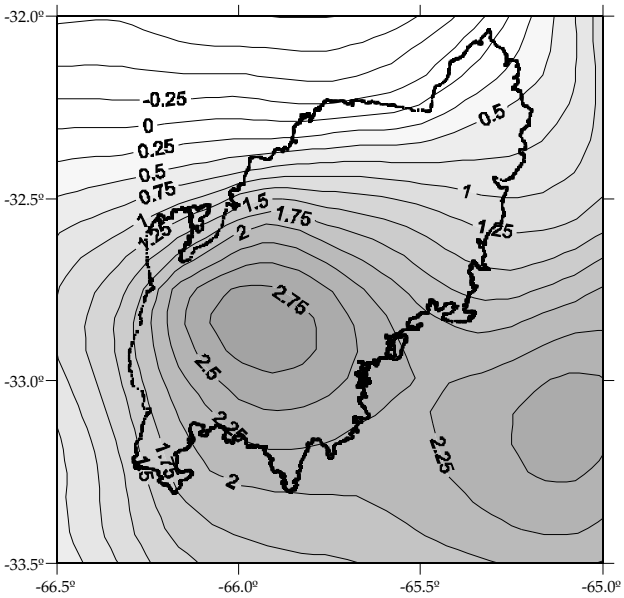

Figure 8. Short wavelenght geoid undulations chart calculated from values in Fig. 7 and equivalent sources method. Contours each 0.25 mGal.

with N_T: total geoid undulations; N_{LWL}: long wavelength geoid undulations, and N_{SWL}: short wavelength geoid undulations. Very short wavelength geoid undulations are not necessary for our geophysical purposes. Geoid undulations N_T calculated here must not be confused with N geoid undulations given by global geopotential models (EIGEN or EGM) with lower resolution power. An expression similar to Eq. 3 was used for free-air anomalies:

$$AAL = AAL_{LWL} + AAL_{SWL} \qquad \textbf{(Eq. 4)}$$

with AAL: total observed free-air anomaly, AAL_{LWL}: long wavelength free-air anomaly, and AAL_{SWL}: short wavelength free-air anomaly. It is well known that in Eq. 3 and Eq. 4, N_{LWL} and AAL_{LWL} are very well defined from global geopotential models (Torge 2001, Introcaso 2006, among others). For calculation of N_{LWL}, we have started from a spherical harmonic expansion of N obtained using both global geopotential models EGM96 and EIGEN CG03C, involving the scale factor N_0 = -53 cm (Lemoine et al. 1998). Both global geopotential models (EGM96 and EIGEN CG03C) are practically identical. Then, we have truncated this spherical harmonic expansion at the following low-degrees: 36, 40, 50 and 70.

Several authors (Doin et al. 1996, Mc Kenzie et al. 1980, Sandwell & Renkin 1988, among others.), have just filtered the spherical harmonic expansion in different empirical low-degrees. In order to calculate N_{SWL} we have used short wavelength free-air anomalies. They were obtained from Eq. 4 with:

$$AAL_{SWL} = AAL - AAL_{LWL} \qquad \textbf{(Eq. 5)}$$

Then, with this gravity anomaly and the equivalent sources method the N_{SWL} chart was defined (Fig. 8); Fig. 5 shows AAL_{LWL} EIGEN CG03C cut in $n = m = 40$ (the step is 1 mGal); Fig. 6 shows N_{LWL} chart from EIGEN CG03C model cut in $n = m = 40$ (the step is 0.25 m); Fig. 7 shows AAL_{SWL} chart (the step is 15 mGal). Proportionality numbers for source depths were assumed following the criterion of Dampney (1969). Varying these numbers we have obtained the results shown in Tables 1-3. Each of them was combined with the spherical harmonic expansion geopotential model truncated at degree and order $n = m = 36$, 40, 50 and 70 for calculation of N_{LWL}. Tables 1-3 show: on the first column $(N_T - N_C) = E$ intervals: [0-0.25] m; [0.25-0.50] m; [0.50-0.75] m and [0.75-1.00] m assumed, with N_T: total geoid undulations obtained from Eq. 3, N_C: geoid undulations from the geometric definition $N_C = h - H$ (order precision approx. ±0.05 m, Fig. 3) and E: residual difference; on the second column the amount of stations for intervals E versus N_{LWL} from the EIGEN CG03C spherical harmonic expansion model truncated at $n = m = 36$, 40, 50 and 70 respectively, and on third column, EGM96 model results.

Tables 1-3 correspond to proportionality factors: 1.4, 2.1 and 2.8 respectively. We have chosen N_{LWL} at $n = m = 40$ from EIGEN CG03C. Fig. 4 shows that results are practically the same thus we have decided to use k = 1.4 following Cordell (1992). Fig. 8 shows the geoid undulations chart corresponding to short wavelengths. It was obtained using free air anomalies (Fig. 7) and the equivalent sources method (step: 0.25 m). Fig. 9 shows the chart of total geoid undulations N_T obtained by adding short wavelength undulations values (Fig. 8) and values obtained using EIGEN CG03C model (Fig. 6) adjusted with eleven $N_C = h - H$ values (step: 0.25 m). The chart of geoid undulations obtained from the global geopotential model EIGEN CG03C is shown in Fig. 10. After comparison of the total geoid undulations chart obtained herein with geoid undulations chart in Fig. 10 (step: 0.25 m) we have found that this later has very poor resolution and different morphology.

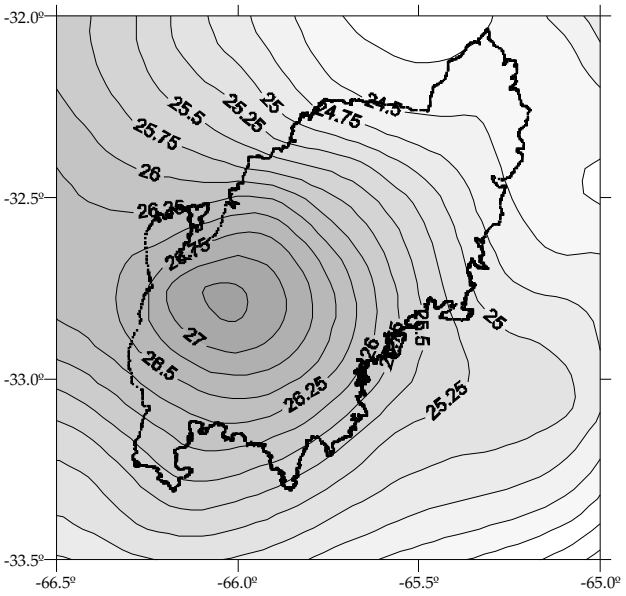

Figure 9. Chart of total geoid undulations N_T of the San Luis range obtained from Fig. 6 chart added to Fig. 8 chart using control stations $N_C = h - H$ in Fig. 3. Contours each 0.25 mGal.

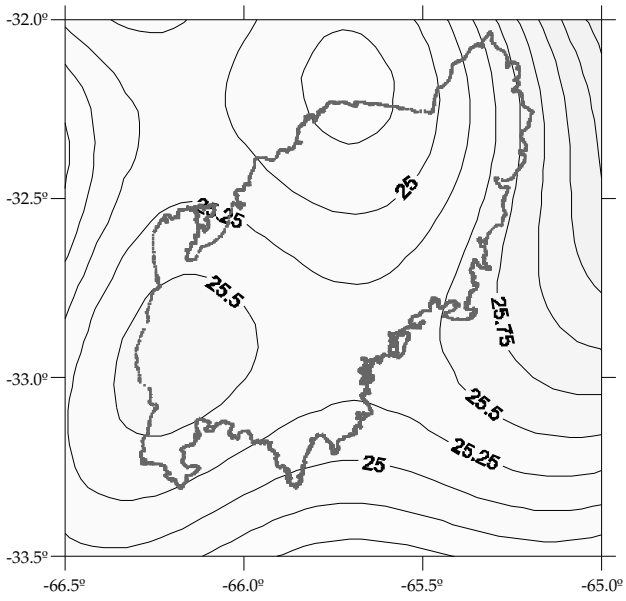

Figure 10. Total geoid undulations chart on the San Luis range obtained from the global geopotential model EIGEN CG03C. Contours each 0.25 mGal.

THEORETICAL COMPARISON MODEL

Ramé & Introcaso (1997) suggested that the San Luis range is apparently compensated in Airy system. In order to analyze the isostatic balance in Airy hypothesis we have prepared an isostatically compensated structural model for the San Luis range, starting with topography as tectonic imput signal (Isacks 1988). We have assumed: a crustal thickness T_N = 33 km (Bullen 1963, Woollard 1969, Introcaso et al. 1992); R (crustal root) = 6.675 H_T with H_T: topographic altitude obtained from altimetry detailed in the data base. This isostatically balanced model (see Fig. 11) was obtained with $H_T + T_N + 6.675\ H_T = T_N + 7.675\ H_T$. In order to calculate the free-air anomalies we have assimilated the topography (Fig. 12) and the corresponding crustal roots as right and homogeneous parallelepipeds. The following equation (Okabe 1979) was employed:

$$g_z(x,y,z) = G\sigma' \left\| x \ln(y+r) + y \ln(x+r) + 2z \arctan \frac{x+y+r}{z} \right|_{\Delta x_1}^{\Delta x_2} \Big|_{\Delta y_1}^{\Delta y_2} \Big|_{\Delta z_1}^{\Delta z_2} \qquad \textbf{(Eq. 6)}$$

being g_z: gravity anomaly (positive effect for H_T and negative effect for R) on stations $E(x, y, z)$. x_i, y_i, z_i: distances between E and the vertices x_1, x_2; y_1, y_2 and z_1, z_2 of parallelepiped i, with $r = [(x_i)^2 + (y_i)^2 + (z_i)^2]^{1/2}$, G: gravitational constant (6.67 x 10^{-8} cm^3 g^{-1} s^{-2}) and ': density of the parallelepiped. Theoretical free-air anomalies were obtained from

$$AAL_{(\text{Theoretical})} = g_{z(\text{Topography})} + g_{z(\text{Crustal root})} \qquad \textbf{(Eq. 7)}$$

Fig. 13 exhibits free-air theoretical anomalies obtained from Eq. 7. There are different methods which can be employed for calculation of the disturbing isostatic potential T from free-air anomalies. For example: Stokes (in Torge 2001, among others), equivalent sources method, or the direct calculation of T (and N) from topography and crustal roots. We have used the equivalent sources method in order to show its versatility. Total geoid undulations involving isostatic effects were calculated using:

$$N_{iT} = N_{LWL} + N_{iLWL} \qquad \textbf{(Eq. 8)}$$

with N_{iT}: total isostatic geoid undulations (Fig. 14) involving N_{iLWL}: local isostatic geoid undulations obtained from theoretical free-air anomalies (Fig. 13) and N_{LWL}: long wavelength geoid undulations (Fig. 6).

Fig. 14 exhibits the total isostatic geoid undulations chart. Fig. 15A shows the location of profile AA' crossing NW-SE the San Luis range and Fig. 15B shows both results on AA' profile: real geoid undulations N_T and geoid undulations involving isostatic balance in Airy hyphotesis N_{iT} which are in good agreement.

CONCLUSIONS

Two geoid undulations charts, N_T and N_{iT}, for the San Luis range were built. Both of them involve long wavelength geoid undulations N_{LWL} obtained by limiting the spherical harmonic expansion to degree and order 40 in the global geopotential model EIGEN CG03C. From observed residual free-air gravity anomalies and using the equivalent sources method we have obtained the geoid undulations chart N_{SWL} that was added to N_{LWL} for defining N_T. The second chart N_{iT} was built from local

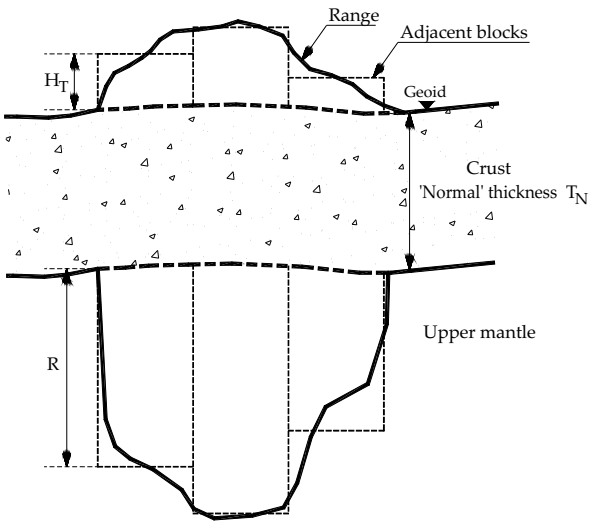

Figure 11. Schematic representation of the Airy isostatic system assumed for the San Luis range.

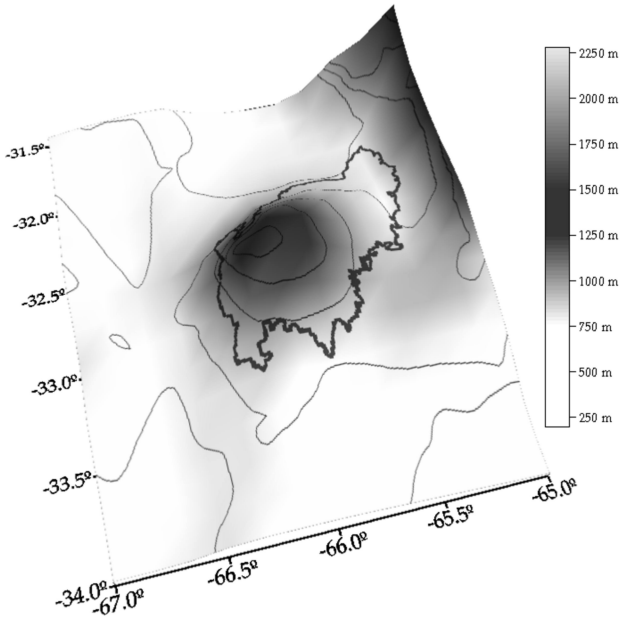

Figure 12. Smoothed topography of the San Luis range and surrounding area. Contours each 250 m.

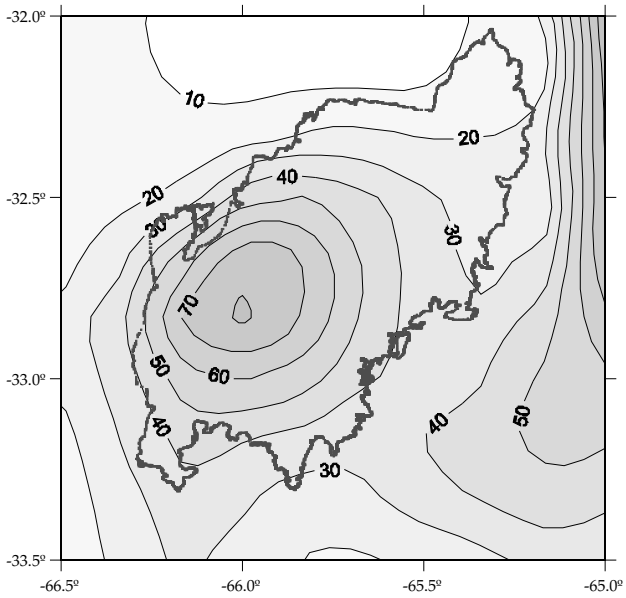

Figure 13. Theoretical free-air gravity anomalies chart (calculated from Eq. 7). Contours each 10 mGal.

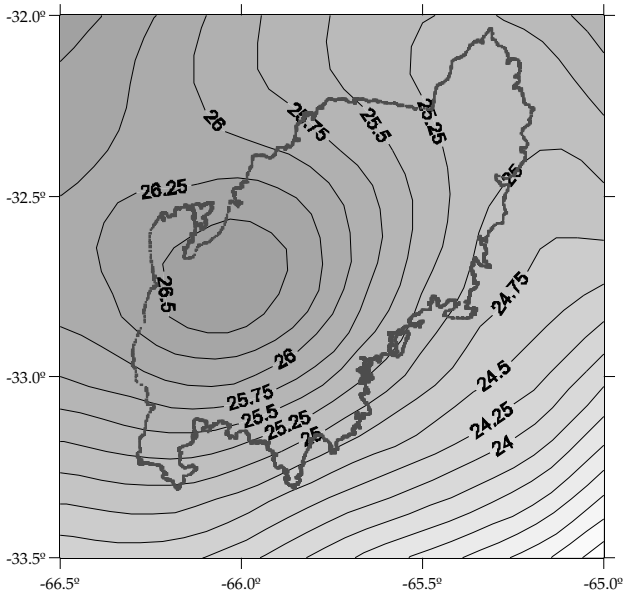

Figure 14. Geoid undulation chart that involves a perfect isostatic balance on the San Luis range. Contours each 0.5 m.

isostatic geoid undulations N_{iLWL} (short wavelenght) obtained from crustal theoretical model in Airy isostatic equilibrium. Thus, $N_{iT} = N_{LWL} + N_{iLWL}$. By comparing both N_T and $N_{i\,T}$ charts and a cross section on the range, we conclude that exists a good consistency between N_T and N_{iT}. Thus, there is a razonable isostatic balance in Airy hyphotesis. We show an alternative method for the analysis of the structural characteristics of the crust.

Acknowledgments

To Gustavo Ramé and Mario Giménez. This work was carried out during the Internal Postdoctoral Scholarship (CONICET) of L.L. Cornaglia. This study has partially been supported by the Agencia Nacional de Promoción Científica y Tecnológica (National Agency of Scienthiphic and Technology Promotion) (PICTR 2002-00166). Graciela Font and an anonymous reviewer contributed for enhancing the manuscript as reviewers of the journal.

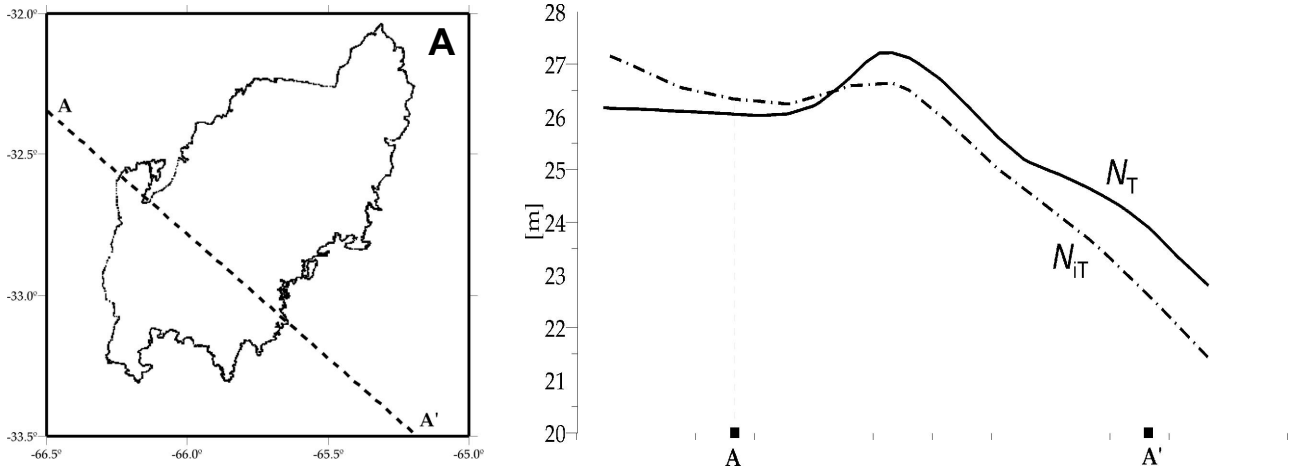

Figure 15. A: Geographic location of the cross section AA' used to compare in 2D geoid undulations from Figs. 9 and 14. **B**. 2D geoid undulations (N_T and N_{iT}) from Figs. 9 and 14 by comparing N_T built from data and $N_{i\,T}$ from isostatically compensated model in Fig. 11, showing good agreement

REFERENCES

Bullen K., 1963. An introduction to the theory of Seismology. Cambridge University Press, Cambridge. 381 p.

Cornaglia L.L., 2005. Determinación del estado isostático y las características corticales de las Sierras de San Luis a partir de las ondulaciones del geoide. Tesis doctoral, Universidad Nacional de Rosario. 133 p. [Unpublished].

Cornaglia L. & Introcaso A., 2004. Exceso de gravedad en al Sierra Grande de San Luis obtenido a partir de ondulaciones del geoide. Estudio preliminar realizado sobre una sección transversal (centrada en 32º50' S). *Geoacta* **29**: 1-9.

Cordell, L. 1992. A scattered equivalent-source method for interpolation and gridding of potencial-field data in three dimensions. *Geophysics* **57(4)**: 629-636.

Criado-Roqué P., Mombrú C. & Ramos V., 1981. Estructura e interpretación tectónica. *In*: Yrigoyen, M. (*Ed.*). Geología de la Provincia de San Luis. *Relatorio del Octavo Congreso Geológico Argentino*: 155-192.

Crovetto C. & Introcaso A., 2004. Indicadores isostáticos geoídicos. Un ejemplo para la sierra de San Luis. *Geoacta* **29**: 49-56.

Dampney C.N.G., 1969. The equivalent source technique. *Geophysics* **34(1)**: 39-53.

Doin M.P., Fleitout L. & McKenzie D., 1996. Geoid anomalies and the structure of continental and oceanic lithospheres. *Journal of Geophysical Research* **101(B7)**: 16119-16135.

Förste C., Flechtner F., Schmidt R., Meyer U., Stubenvoll R., Barthelmes F., König R., Neumayer K.H., Rothacher M., Reigber C., Biancale R., Bruinsma S., Lemoine J.-M. & Raimondo J.C., 2005. A New High Resolution Global Gravity Field Model Derived From Combination of GRACE and CHAMP Mission and Altimetry/Gravimetry Surface Gravity Data. *Poster presented at EGU General Assembly 2005 (April), Vienna, 24-29*.

Guspí F., Introcaso A. & Pacino M.C., 1995. Carta gravimétrica argentina 1995: su construcción. *Actas Congreso Argentino de Geociencias y Geotectónicas & Noveno Congreso Nacional de Cartografía,* Buenos Aires, Centro Argentino de Cartografía **1**: 88-93.

Guspí F., Introcaso A. & Introcaso B., 2004. Gravity-enhanced representation of measured geoid undulations using equivalent sources. *Geophysical Journal International (RAS)* **158**: 1-8.

Introcaso A., 2004. Ambigüedad en la inversión del campo potencial. Sus ventajas para la obtención del geoide local. *Tópicos de Geociencias* (Editorial Fundación Universidad Nacional de San Juan): 255-267.

Introcaso A., 2006. Geodesia Física. *Boletín del Instituto de Fisiografía y Geología* **Vol. Especial 1**: 1-128.

Introcaso A., Pacino M.C. & Fraga H., 1992. Gravity, isostasy and Andean crustal shortening between latitudes 30ºS and 35ºS. *Tectonophysics* **205**: 31-48.

Introcaso A. & Crovetto C., 2005. Introducción a la construcción del geoide. *Temas de geociencia* **12**: 1-56.

Isacks B., 1988. Uplift of the central Andean Plateau and bending of the Bolivian Orocline. *Journal of Geophysical Research* **93(B4)**: 3211-3231.

Jordan T.E. & Allmendinger R.W., 1986. The Sierras Pampeanas of Argentina: A modern analogue of rocky mountain foreland deformation. *American Journal of Science* **286**: 737–764.

Lemoine F., Kenyon S., Factor J., Trimmer R., Pavlis N., Chiuw D., Cox C., Klosko S., Lutheke S., Torrence M., Wang Y., Williamson R., Pavlis H., Rapp R. & Olson T., 1998. The development of the joint NASA, CSFC and NIMA geopotential model EGM96, NASA/TP, 1998 – 206861, Goddard Space Flight Center.

McKenzie D., Watts A., Pearson B. & Roufosse M., 1980. Platform and mantle convection beneath the Pacific Ocean. *Nature* **288**: 442-446.

Okabe M., 1979. Analytical expressions for gravity anomalies due to homogeneous polyhedral bodies and translations into magnetic anomalies. *Geophysics* **44(4)**: 730-741.

Ramé G. & Introcaso A., 1997. Análisis isostático

preliminar de la Sierra Grande de San Luis, Argentina. *Revista de la Asociación Geológica Argentina* **53(3)**: 379-386.

Sandwell D. & Renkin M.L., 1988. Compensation of swells and plateaus in the North Pacific. *Journal of Geophysical Research* **93(B4)**: 2775-2783.

Sato A.M., Gonzalez P.D. & Llambías E.J., 2003. Evolución del orógeno Famatiniano en la Sierra de San Luis: magmatismo de arco, deformación y metamorfismo de bajo a alto grado. *Revista de la Asociación Geológica Argentina* **58(4)**: 487-504.

Torge W., 2001. Geodesy (3rd edition). *Walter de Gruyter*. Berlin-New York. 416 p.

Woollard G., 1969. Regional Variations in Gravity. Geophysical Monograph. *American Geophysical Union* **13**: 320-341.

PASOTTIA, A NEW GENUS OF TITHONIAN OPPELIID AMMONITES (LATE JURASSIC, AMMONOIDEA: HAPLOCERATOIDEA)

Horacio PARENT, Günter SCHWEIGERT, Armin SCHERZINGER & Raymond ENAY

Boletín del Instituto de Fisiografía y Geología

Parent H., Schweigert G., Scherzinger A. & Enay R., 2008. *Pasottia*, a new genus of Tithonian oppeliid ammonites (Late Jurassic, Ammonoidea: Haploceratoidea). *Boletín del Instituto de Fisiografía y Geología* **78(1-2)**: 23-30. Rosario, 02-12-2008. ISSN 1666-115X.

Abstract.- Extensive sampling in recent years of the Tithonian ammonite fauna of the Neuquén-Mendoza Basin has yielded samples of a new oppeliid genus which is herein described under the name *Pasottia* n. gen. with *Pasottia andina* n. sp. as the type-species. The holotype comes from the Middle Tithonian Zitteli Zone of La Amarga, southern Neuquén-Mendoza Basin. *P. andina* n. sp. is recorded from La Amarga and Cerro Lotena, confined to a single horizon of the Zitteli Zone. *Pasottia* n. gen. is classified in the Subfamily Taramelliceratinae based on (1) the characteristic microconch with a well marked sulcus with a row of linguiform structures on middle flank of last whorl of phragmocone and bodychamber, which is geniculate and (2) the unkeeled, narow rounded venter of both sexual dimorphs. Based on the ammonite assemblage of the type horizon is dated in the Semiforme Zone of the Primary International Standard.

Key-words: Ammonoidea; Oppeliidae; *Pasottia andina* n.gen. et n. sp.; Middle Tithonian; Andes; Argentina.

Resumen.- ***Pasottia*, un nuevo género de amonites tithonianos de la famlia Oppeliidae (Jurásico Tardío, Ammonoidea: Haploceratoidea).** Extensos muestreos de la fauna de amonites tithonianos de la Cuenca Neuquén-Mendoza realizados en los últimos años han puesto en evidencia la ocurrencia de un nuevo género descripto como *Pasottia* n. gen., con *Pasottia andina* n. sp. como su especie tipo. El holotipo proviene de la Zona Zitteli del Tithoniano Medio de La Amarga, localidad del extremo sur de la cuenca. *P. andina* n. sp. ha sido registrada en su localidad tipo y en Cerro Lotena, confinada en un horizonte de la parte media de la Zona Zitteli. *Pasottia* n. gen. es incluído en la subfamilia Taramelliceratinae sobre la base de: (1) la característica microconcha que posee un marcado surco con una fila de estructuras linguiformes en la mitad del flanco de la última vuelta del fragmócono y la cámara habitacional, la cual es geniculada, y (2) ambos dimorfos sexuales poseen un vientre estrecho y redondeado, sin quilla. Sobre la base del conjunto de amonites asociados en el horizonte tipo se concluye que éste es de edad Zona Semiforme del estándar primario interenacional.

Palabras clave: Ammonoidea; Oppeliidae; *Pasottia andina* n. gen. et n. sp.; Tithoniano Medio; Andes; Argentina.

Horacio Parent [e-mail: parent@fceia.unr.edu.ar]: *Laboratorio de Paleontología, FCEIA, Universidad Nacional de Rosario, Pellegrini 250, 2000 Rosario, Argentina.*

Günter Schweigert [e-mail: schweigert.smns@naturkundemuseum-bw.de]: *Staatliches Museum für Naturkunde, Rosenstein 1, 70191 Stuttgart, Germany.*

Armin Scherzinger [e-mail: armin.scherzinger@hotmail.de]: *Hewenstraße 9, 78194 Immendingen-Hattingen, Germany.*

Raymond Enay [e-mail: Raymond.Enay@univ-lyon1.fr]: *UFR Sciences de la Terre, Université Claude Bernard - Lyon 1, 43 bd du 11 Novembre, 69622 Villeurbanne cedex, France.*

Received: 10/06/2008; accepted: 20/08/2008.

Editors: E. P. Peralta and A.F. Greco

INTRODUCTION

The Tithonian ammonoid fauna of the Neuquén-Mendoza Basin (NMB) has been studied for a long time (see Leanza 1981 and Parent 2003 for references). Nevertheless publication has been slow and does not clearly reflect the true diversity of the ammonoids that are present. The descriptions of the Haploceratoidea are particularly sparse. Among recent papers the most comprehensive description (Leanza 1980) includes five species: *Pseudolissoceras zitteli* (Burckhardt, 1903), *P. pseudoolithicum* (Haupt, 1907), *Parastreblites comahuensis* Leanza, 1980, *Glochiceras steueri* Leanza, 1980 and *Hildoglochiceras wiedmanni* Leanza, 1980. Extensive sampling in recent years of the Tithonian of the southern and central NMB has revealed a higher diversity. There are several new forms, some of which, if in small samples or poorly preserved adult specimens, are hard to distinguish from *P. zitteli*. In the Zitteli Zone of Cerro Lotena and La Amarga, two localities in the southern NMB (Fig. 1), an oppeliid genus occurs rather abundantly that has not been previously described.

The objective of this paper is to describe this new genus and the new species on which it is based.

STRATIGRAPHIC FRAMEWORK

All the material presented in this paper was collected at La Amarga and Cerro Lotena. The Tithonian of these two localities is represented by marine rocks of the Vaca Muerta Fm., conformably overlying the conspicuous conglomerates and coarse sandstones of the Tordillo Fm. At the base of the Lower Tithonian the lowermost Mendozanus Zone is represented mostly by fine to coarse sandstones that contain abundant, sometimes moderately well-preserved ammonites of the earliest Andean Tithonian faunal horizon, provisionally named "Fauna A" (Parent et al. 2006). Upwards, to the base of the Zitteli Zone, the base of the Middle Tithonian, there follow several meters of marls with a still undescribed fauna of perisphinctids. The Zitteli Zone consists mainly of a succession of shales and marls, partially covered, which can be subdivided into three parts (the faunal lists below are not exhaustive, only the most representative taxa are mentioned):

(1) the lower part (6-10 m): gray to yellowish shaly marls with abundant nodules containing *Pseudolissoceras zitteli*, and representatives of *Choicensisphinctes* Leanza, 1980, "*Lithacoceras*" Hyatt, 1900, *Catutosphinctes* Leanza & Zeiss, 1992 and micro- and macroconch aspidoceratids.

(2) the middle part (about 1 m): gray shaly marls with large nodules and an abundant ammonite fauna: *P. zitteli*, *Pasottia andina* n. gen. et n. sp., *G. steueri* (microconch of an undescribed genus widely represented through the Lower and Middle Tithonian of the basin), *Choicensisphinctes*, *Catutosphinctes*, and macro- and microconch aspidoceratids (including "*H. wiedmanni*", see below).

(3) the upper part (3-10 m, best exposed at La Amarga): brown, hard limestones and marls with large nodules and an abundant ammonite fauna: *P. zitteli*, *G. steueri*,

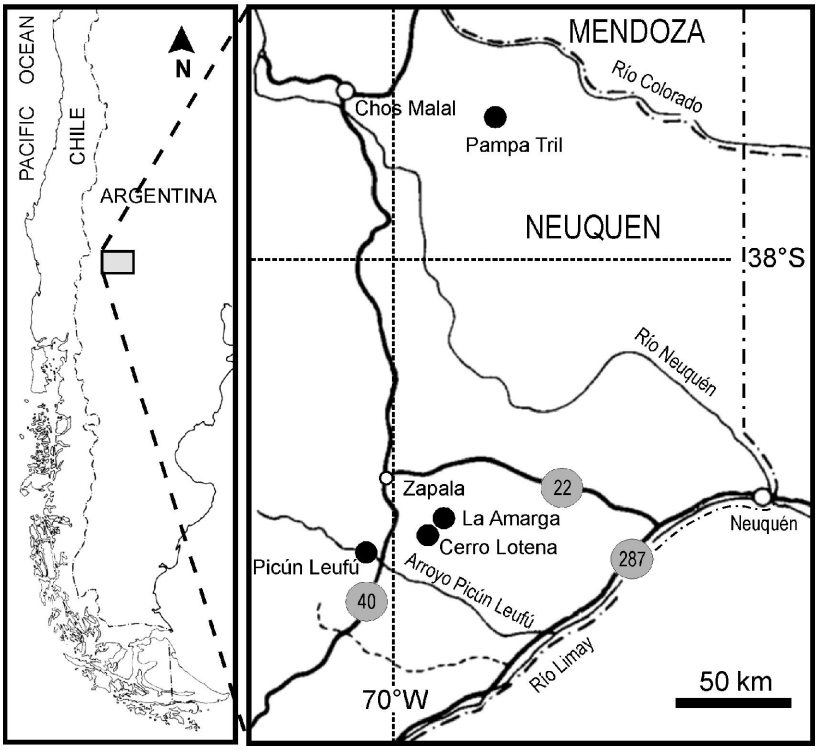

Figure 1. Map showing the localities cited in the text.

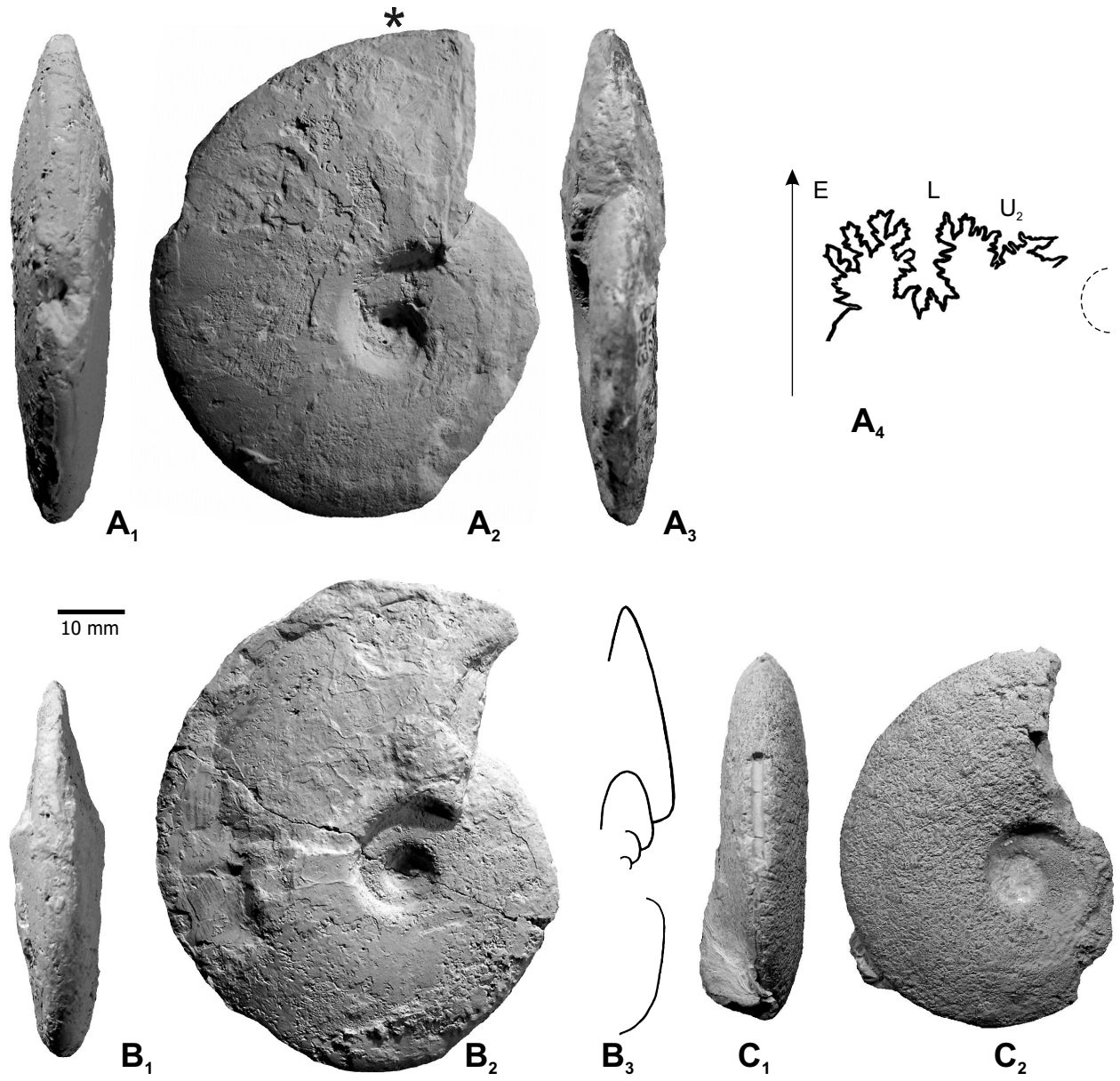

Figure 2. *Pasottia andina* n. gen. et n. sp. **A**: holotype (LPB 853), complete adult macroconch phragmocone with incipient bodychamber, ventral (**A**$_1$), lateral (**A**$_2$) and apertural (**A**$_3$) views and last septum suture line (**A**$_4$); La Amarga; Zitteli Zone. **B**: paratype (LPB 1090) complete adult macroconch phragmocone, ventral (**B**$_1$) and lateral views (**B**$_2$) and whorl section (**B**$_3$); Cerro Lotena; Zitteli Zone. **C**: paratype (LPB 1090/1), incomplete adult macroconch phragmocone, ventral (**C**$_1$) and lateral (**C**$_2$) views; La Amarga; Zitteli Zone. All natural size excepted suture (**A**$_4$) x3. - Asterisk at last septum.

Choicensisphinctes, *Catutosphinctes*, *Volanoceras krantzense* Cantú-Chapa, 1990, *Physodoceras* cf. *neoburgense* (Oppel, 1863) and other macro- and microconch aspidoceratids (including "*H. wiedmanni*"). Most likely this part of the section includes the horizon from which the holotype of *P. comahuensis* was collected (Bed 5 in Leanza 1980: 9).

This upper part is followed by a succession of poorly fossiliferous, bluish to greenish shales, gray siltstones and mudstones, which in Cerro Lotena pass into marls and limestones containing, mainly in their upper part, an abundant fauna of the Proximus Zone, including oppeliids, *Catutosphinctes*, and aspidoceratids.

SYSTEMATIC PALEONTOLOGY

The studied material is housed in the Museo Olsacher (MOZP), Zapala, Neuquén and in the Laboratorio de Paleontología (LPB), Universidad Nacional de Rosario. Macroconch (female): [M]; microconch (male): [m]. Dimensions are as follows: diameter (*D*), diameter at last septum (D_{ls}), diameter at adult peristome (D_p), umbilical width (*U*), width of whorl section (*W*), height of whorl section (H_1), and ventral or apertural height of whorl section (H_2), all given in millimeters (mm); approximated values denoted by (^{e}). OD: original designation; SD: subsequent designation; TS: type species.

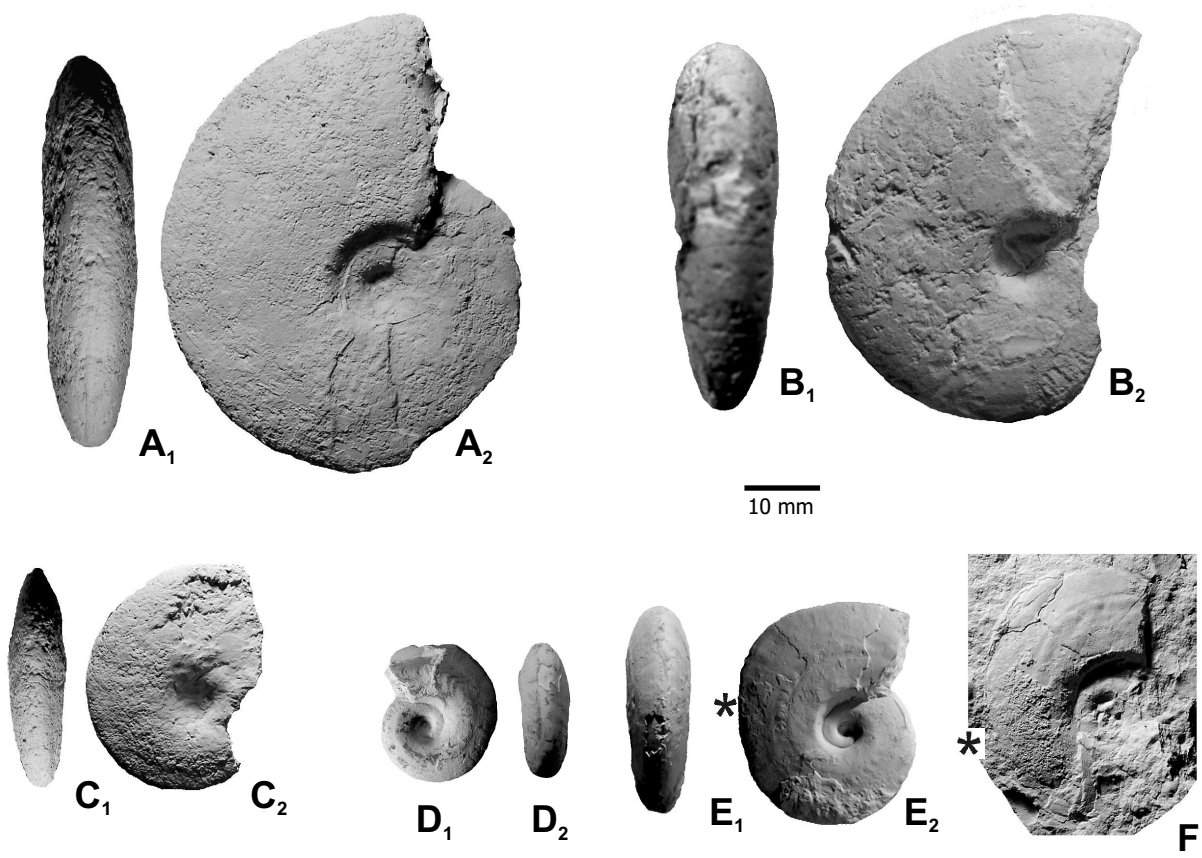

Figure 3. *Pasottia andina* n. gen. et n. sp. **A**: paratype (LPB 1090/2), adult macroconch phragmocone, ventral (**A**$_1$) and lateral (**A**$_2$) views; La Amarga; Zitteli Zone. **B**: paratype (MOZP 6870/2) adult macroconch phragmocone, ventral (**B**$_1$) and lateral views (**B**$_2$); La Amarga; Zitteli Zone. **C**: paratype (LPB 936), inner whorls of a macroconch, ventral (**C**$_1$) and lateral (**C**$_2$) views; La Amarga; Zitteli Zone. **D**: paratype (MOZP 7535/2), adult microconch phragmocone, lateral (**D**$_1$) and ventral (**D**$_2$) views; Cerro Lotena; Zitteli Zone. **E**: paratype (MOZP 7535/1), almost complete adult microconch,ventral (**E**$_1$) and (**E**$_1$) lateral views; Cerro Lotena, Zitteli Zone. **F**: paratype (MOZP 6853), almost complete adult microconch, lateral view; La Amarga; Zitteli Zone. - All natural size. Asterisk at last septum.

Superfamily Haploceratoidea Zittel, 1884
Family Oppeliidae H. Douvillé, 1890
Subfamily Taramelliceratinae Spath, 1928
Genus *Pasottia* n. gen.

Type species.- *Pasottia andina* n. sp. (description below).

Derivatio nominis.- In honour of the late Pierina E. Pasotti who made important contributions in Geology and Paleontology, and encouraged and supported ammonite research when directing the Instituto de Fisiografía y Geología (FCEIA – UNR).

Diagnosis.- Macroconch smooth, compressed suboxycone with high ovate to subtriangular whorl section; phragmocone moderately involute with rounded umbilical shoulder passing to uncoiled with sharp umbilical shoulder and flat, sloping wall. Bodychamber becoming strongly contracted, the umbilical seam uncoiled. Microconch inner whorls like in the macroconch; bodychamber also strongly contracted, geniculate from a point at which the rounded umbilical shoulder of the phragmocone becomes sharp and the umbilical wall flat and sloping. Last whorl of phragmocone and bodychamber with a sulcus and a dense row of linguiform structures.

Remarks and comparisons.- Inclusion in the subfamily Taramelliceratinae rather than in Streblitinae Spath, 1925 is indicated by (1) the microconch which has a lateral sulcus with a well marked row of linguiform structures, and (2) the venter which although narrow and smooth, lacks any kind of keel. It is worth remarking that some Streblitinae have a hollow floored keel which can be observed only in well preserved specimens. This is the case in *Uhligites* Kilian, 1913 (TS: *Streblites kraffti* Uhlig, 1903; SD by Roman 1938) as noted by Uhlig (1903: 34, 45) and confirmed with recently collected material from Southern Tibet (cf. Yin & Enay 2004).

Microconchs of the Haploceratidae Zittel, 1884 have smooth flanks and rounded umbilical shoulders, and those of *Haploceras* Zittel, 1870 (TS: *Ammonites elimatus* Oppel, 1865; SD by Spath 1923) have ventral crenulation (see Enay & Cecca 1986 and Wright et al. 1996).

Among the haploceratids genera known in the NMB the most closely similar is *Pseudolissoceras* Spath, 1925 (TS: *Neumayria zitteli* Burckhardt, 1903; OD). The macroconchs of *Pasottia* n. gen. can be easily distinguished from those of *Pseudolissoceras* spp. by the consistently smaller adult size and more compressed, suboxyconic shell shape. Moreover, the septal suture line of *Pasottia* n. gen. is significantly more incized, especially in its first lateral lobe which is trifurcated. The

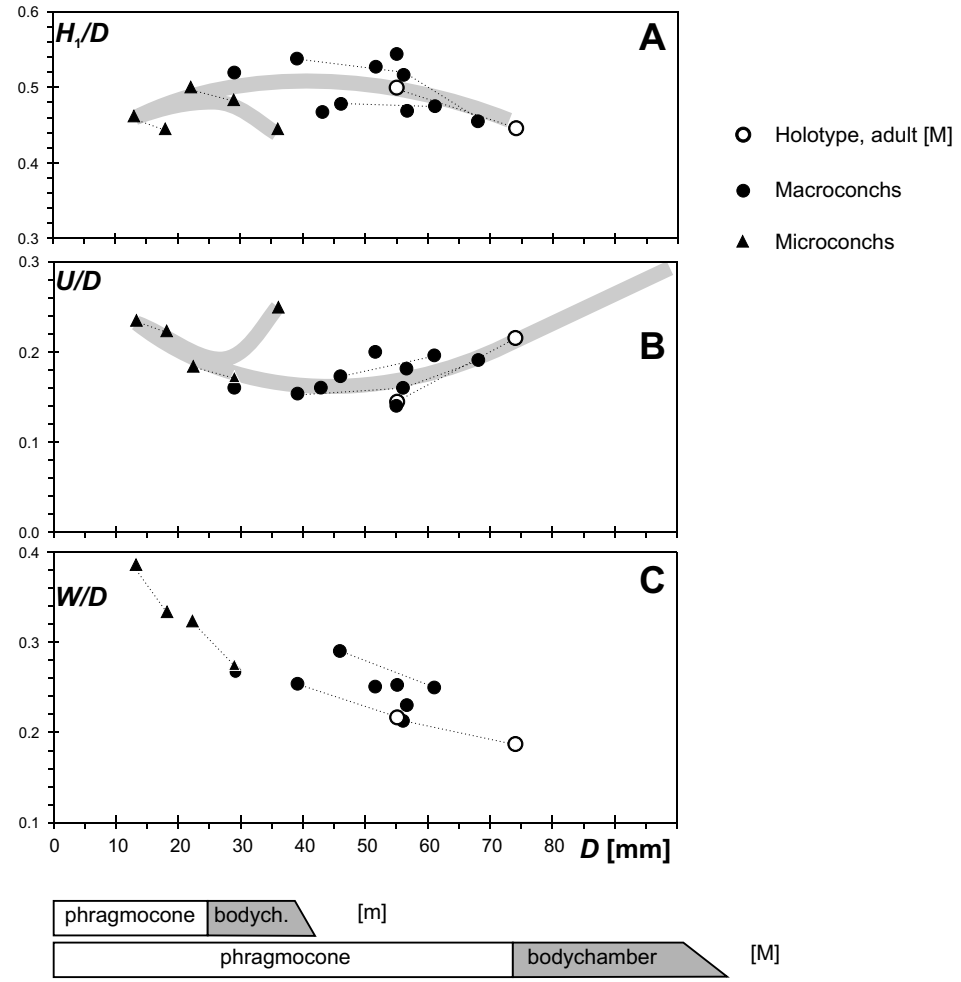

Figure 4. *Pasottia andina* n. gen. et n. sp. [M&m]. Relative dimensions versus diameter, ontogenetic trajectories and indication of phragmocone and bodychamber lengths for both sexual dimorphs. **A**: H_1/D - *D*. **B**: *U*/*D* - *D*. **C**: *W*/*D* - *D*. Thin broken lines linking multiple observations from a single specimen. Thick shaded curves illustrating the sexually dimorphic ontogenetic trajectories.

microconchs are also very different: in *Pasottia* n. gen. they are somewhat stouter and their bodychamber is geniculate from a point of ontogeny at which the well rounded, indistinct umbilical shoulder becomes suddenly sharp and almost rectangular. Another important difference between the microconchs is the completely smooth shell in *Pseudolissoceras* (see Parent 2001: fig. 7C-D), compared with a well-marked sulcus and a row of linguiform structures from the last whorl of the phragmocone in *Pasottia* n. gen.

***Pasottia andina* n. sp.**

Figs. 2-4; Table 1

Holotype.- The specimen LPB 853 (Fig. 2A), an adult macroconch phragmocone with beginning of the bodychamber preserved.

Paratypes.- Nine macroconchs (La Amarga: LPB 854-855, 936, 1090/1-4, MOZP 6870/2; C. Lotena: LPB 1090) and three microconchs (La Amarga: MOZP 6853; C. Lotena: MOZP 7535/1-2). All specimens of La Amarga come from the type horizon; those of Cerro Lotena come from biostratigraphically equivalent beds.

Type locality and horizon.- La Amarga, southern Neuquén Province (Fig. 1). Zitteli Zone, Andean Middle Tithonian; Vaca Muerta Fm.

Derivatio nominis.- Trivial name is derived from the Andean Chain.

Description.- Holotype (Fig. 2A): smooth suboxyconic adult macroconch phragmocone retaining small portion of the bodychamber; D_{ls} = 74 mm. Inner whorls compressed suboval, higher than wide with rounded umbilical shoulder. Umbilicus on last whorl of phragmocone widely uncoiled, whorl section subtriangular, very narrow venter, weakly convex flanks and sharp umbilical shoulder passing to a flat sloping wall. Remains of the umbilical seam indicate a final diameter at the terminal adult peristome (D_p) of at least 100 mm, with a bodychamber of not less than a half whorl.

Macroconchs (Figs. 2A-C, 3A-C): All available material consists of phragmocones; the bodychamber is known only partially from poorly preserved, crushed, unfigured remains. The specimen LPB 936 (Fig. 3C) shows the distinctive inner whorls, very compressed with a small umbilicus. There is little variation in adults and

Table 1. *Pasottia andina* n. gen. et n. sp. Dimensions of the holotype and paratypes. Bc: bodychamber; Ph: phragmocone; Ad: adut; Juv: juvenil.

		D	*U*	*U/D*	*W*	*W/D*	H_1	H_1/D	W/H_1	H_2	H_2/D
Macroconchs											
LPB 853 holotype	Bc/Ad	74.00	16.00	0.22	14.00	0.19	33.00	0.45	0.42	24.00	0.44
	Ph/Ad	55.00	7.50	0.14	12.00	0.22	27.50	0.50	0.44	23.00	0.42
LPB 1090	Ph/Ad	68.00	13.00	0.19	–	–	31.00	0.46	–	20.00	0.29
		56.00	9.00	0.16	12.00	0.21	29.00	0.52	0.41	–	–
LPB 1090/2	Ph/Ad	61.00	12.00	0.20	15.30	0.25	29.00	0.48	0.41	20.00	0.33
		46.00	8.00	0.17	13.30	0.29	22.00	0.48	0.41	–	–
		39.00	6.00	0.15	10.00	0.26	21.00	0.54	0.48	–	–
MOZP 6870/2	Ph/Ad	55.00	7.50	0.14	14.00	0.25	30.00	0.55	0.47	–	–
LPB 1090/4	Ph/Ad	51.50	10.10	0.20	13.00	0.25	27.20	0.53	0.48	–	–
		43.00	7.00	0.16	–	–	20.10	0.47	–	–	–
LPB 936	Ph/Juv	29.00	4.50	0.16	7.80	0.27	15.10	0.52	0.52	–	–
LPB 1090/1	Ph/Ad	56.50	10.20	0.18	12.80	0.23	26.50	0.47	0.48	–	–
Microconchs											
MOZP 6853	Bc/Ad	36.00(e)	9.00(e)	0.25(e)	–	–	16.00	0.44	–	9.00	0.25
MOZP 7535/1	Bc/Ad	29.00	5.00	0.17	8.00	0.28	14.00	0.48	0.57	9.00	0.31
	Ph/Ad	22.00	4.00	0.18	7.00	0.32	11.00	0.50	0.64	–	–
MOZP 7535/2	Ph/Ad	18.00	4.00	0.22	6.00	0.33	8.00	0.44	0.75	–	–
		13.00	3.00	0.23	5.00	0.38	6.00	0.46	0.83	–	–

subadults in comparison with the holotype (Fig. 4). Some specimens are slightly more inflated with a somewhat wider venter, especially the specimen MOZP 6870/2 (Fig. 3B). The diameter of the siphuncule in the specimen LPB 1090/1 (Fig. 2C) is 1.3 mm at $D = 47$ mm.

Microconchs (Fig. 3D-F): Innermost whorls ($D <$ 5 mm) depressed suboval and smooth. Subsequent whorls of phragmocone show a trend towards suboval higher than wide, with a rounded umbilical shoulder. The last whorl of the adult phragmocone, from about $D = 10$-15 mm, carries a sulcus, with a row of linguiform structures that are somewhat reinforced all along the bodychamber. Close to the beginning of the bodychamber ($D = 25$ mm) there occurs a sudden change to a subtrapezoidal whorl section with rounded venter, subplanar flanks and a sharp umbilical shoulder passing down into a steeply sloping wall. Bodychamber uncoiled.

Remarks and comparisons.- Fig. 4 illustrates the described ontogenetic changes of relative dimensions of the juvenil and adult stages of both sexual dimorphs.

Some specimens of *P. zitteli* associated with *P. andina* n. sp., both in Cerro Lotena and La Amarga, are somewhat similar in their sharp umbilical shoulders and sloping walls but their larger adult size and other differences - sutural degree of incision and oxyconic shape - discussed above at the generic level, make possible a rather clear separation.

Pseudolissoceras concorsi Donze & Enay, 1961 [M] and *Pseudolissoceras bavaricum* Barthel, 1962 [M] have flanks with a well marked periumbilical concavity or depression and very simple septal suture line, with ceratitic aspect (discussion in Parent 2001). These two traits strongly differentiate *P. andina* n. sp., which shows more complex septal suture and the maximum width of whorl section just on the umbilical shoulder.

P. comahuensis is known only by its holotype, a phragmocone from Cerro Lotena which differs from *P. andina* n. sp. in its larger adult size and more inflated last whorl with a much narrower umbilicus. "*Neochetoceras*" sp. from the Lower Tithonian Mendozanus Zone of the NMB (Parent et al. 2006) differs from *Pasottia* n. gen. by the occurrence of falcoid ribs, a rounded umbilical shoulder and a different cross-section.

Placenticeras fallax Castillo & Aguilera, 1895 (holotype refigured by Verma & Westermann 1973: pl. 29: 2) from Mexico, resembles *P. andina* n. sp. in its sharp umbilical shoulder, involution and adult size, but differs in the somewhat more inflated last preserved whorl. The species was assigned to *Haploceras* by Verma & Westermann (1973) but most likely belongs to *Pasottia* n. gen.

Glochiceras somalicum Spath, 1925, a microconchiate oppeliid from the ?Kimmeridgian of Somalia, has a lateral sulcus with a row of linguiform structures and a sharply defined steep umbilical edge, but differs in its wider umbilicus and the bodychamber uniformly uncoiled, not geniculate as in *P. andina* n. sp.

The holotype of *"Hildoglochiceras" wiedmanni* Leanza has tuberculate inner whorls (see Leanza 1980: pl. 1: 4), and several complete specimens with lappets collected recently in Cerro Lotena and La Amarga indicate that this ammonite is in fact a microconch aspidoceratid, very close if not identical with *"Glochiceras" parabolistriatum* Krantz, 1926. "*Hildoglochiceras" nudum* Collignon, 1960, a microconchiate oppeliid from Madagascar known only by its holotype, said to come from the Kobelli Zone, is somewhat similar to microconch *P. andina* n. sp. in shell shape but differs in that the lateral sulcus is narrower and it shows some kind of weak ribs or growth lines in the outer half of the flanks.

Distribution.- Well represented in La Amarga and C. Lotena (southern NMB), with a few specimens collected in

Picún Leufú (southern NMB), Pampa Tril (Fig. 1) and Arroyo Cieneguita (central NMB).

Age.- Middle part of the Zitteli Zone, Andean lower Middle Tithonian. In La Amarga, *P. andina* n. sp. occurs just below a recently collected well-horizoned fauna that includes *P. zitteli*, *V. krantzense* and *P*. cf. *neoburgense*. This association may be correlated with the Semiforme Zone of the Primary International Standard (see Schweigert et al. 2002). Thus, it may be assumed that the type horizon of *P. andina* n. sp. is Semiforme Zone in age (early Middle Tithonian) or older. The underlying horizon in the studied sections yields the first *P. zitteli*. This species and its total range biozone are commonly accepted as restricted to the Semiforme Zone (see Parent 2001). In this context it is concluded that the type horizon of *P. andina* is Semiforme Zone in age.

CONCLUSION

In the Zitteli Zone of Cerro Lotena and La Amarga (southern Neuqúen-Mendoza Basin) occurs rather abundantly *Pasottia andina* n. gen. et n. sp. The new oppeliid genus belongs to the Taramelliceratinae and is strongly sexually dimorphic. The new species is very similar to the co-occurrent, abundant *Pseudolissoceras zitteli*, from which can be clearly differentiated by the more incized septal suture line with the first lateral lobe trifurcated, the smaller adult size of the macroconchs and the different sexual dimorphism.

The consistent occurrence confined to a single horizon in C. Lotena and La Amarga, and some few records from biostratigraphically equivalent levels in Picún Leufú, Pampa Tril and Arroyo Cieneguita, suggests that *P. andina* n. sp. could be a good guide fossil.

Acknowledgements
Sergio E. Cocca, Rafael Cocca, Javier Chávez (Zapala), Oscar D. Capello, Sofía Parent and Julieta Parent (Rosario) gave valuable assistance in the field. Adrián Pellegrini and Mario Pellegrini (Rosario) gave valuable technical support in laboratory. Gerard Delanoy (Nice) kindly provided literature. J.H. Callomon (London), A.B. Villaseñor (México) and A. Zeiss (Erlangen) have made valuable suggestions to improve the manuscript as reviewers of the journal.

REFERENCES

Barthel K.W., 1962. Zur Ammonitenfauna und Stratigraphie der Neuburger Bankkalke. *Bayerische Akademie der Wissenschaften, Mathematisch-naturwissenschaftliche Klasse* **105**: 1-30.

Burckhardt C., 1903. Beiträge zur Kenntnis der Jura- und Kreideformation der Cordillere. *Palaeontographica* **50**: 1-145.

Cantu-Chapa A., 1990. *Volanoceras chignahuapense* sp. nov., amonita del Titoniano Inferior de Puebla, Centro de México. *Revista Sociedad Mexicana de Paleontología* **3(1)**: 41-45.

Castillo A. del & Aguilera J.G., 1895. Fauna fósil de la Sierra de Catorce. *Boletín de la Comisión geológica de México* **1**: 1-55.

Collignon M., 1960. Atlas des fossiles characteristiques de Madagascar. Fascicule 6 (Tithonique). *Service Geologique de Madagascar, Tananarive.* Plates 134-175.

Donze P. & Enay R., 1961. Les Céphalopodes du Tithonique Inferieur de la Croix-de-Saint-Concors pres Chambéry (Savoie). *Travaux Laboratoire Géologique de Lyon NS* **7**: 1-236.

Douvillé H., 1890. Sur la classification des Cératites de la Craie. *Bulletin de la Societé Geologique de France (serie 3)* **18** : 275-292.

Enay R. & Cecca F., 1986. Structure et evolution des populations tithoniques du genre d'ammonites téthysien *Haploceras* Zittel, 1868. *In* G. Pallini, F. Cecca, S. Cresta, M. Santantonio (*eds*.): Atti del primo convegno internazionale Fossili, Evoluzione, Ambiente, Pergola 1984: 37-53.

Haupt O., 1907. Beiträge zur Fauna des oberen Malm und der unteren Kreide in der argentinischen Cordillere. *Neues Jahrbuch für Mineralogie, Geologie und Paläontologie, Beilage-Band* **21**: 187-236.

Hyatt A., 1900. Cephalopoda. *In*: Zittel K.A.: Textbook of Palaeontology, 1st English ed. (transl. by C.R. Eastman): 502-592. Mcmillan London & New York.

Kilian C.C.C.W., 1907-1913. Erste Abteilung: Unterkreide (Palaeocretacicum). Lieferung 1-3: 1-398. *In* F. Frech: Lethaea Geognostica. II. Das Mesozoicum, Band 3 (Kreide). Schweizerbart. Stuttgart.

Krantz F., 1926. Die Ammoniten des Mittel- und Obertithons. *In*: Jaworski E., Krantz F. & Gerth H. (*eds.*): Beiträge zur Geologie und Stratigraphie des Lias, Doggers, Tithons und der Unterkreide im Süden der Provinz Mendoza (Argentinien). *Geologische Rundschau* **17a**: 427-462.

Leanza H.A., 1980. The Lower and Middle Tithonian ammonite fauna fom Cerro Lotena, province of Neuqúen, Argentina. *Zitteliana* **5**: 3-49.

Leanza H.A., 1981. The Jurassic-Cretaceous boundary beds in West Central Argentina and their ammonite zones. *Neues Jahrbuch für Geologie und Paläontologie, Abhandlungen* **161(1)**: 62-92.

Leanza H.A. & Zeiss A., 1992. On the ammonite fauna of the Lithographic Limestones from the Zapala region (Neuquén province, Argentina), with the description of a new genus. *Zentralblatt für Geologie und Paläontologie, Teil I*, **Heft 6, 1991**: 1841-1850.

Oppel A., 1862-1863. III. Über jurassische Cephalopoden. *Paleontologische Mittheilungen aus dem Museum des koeniglich Bayerischen Staates* **1**: 127-262.

Parent H., 2001. The Middle Tithonian (Upper Jurassic) ammonoid fauna of Cañadón de los Alazanes, southern Neuqúen-Mendoza Basin, Argentina. *Boletín del Instituto de Fisiografía y Geología* **71(1-2)**: 19-38.

Parent H., 2003. The ataxioceratid ammonite fauna of the Tithonian (Upper Jurassic) of Casa Pincheira, Mendoza (Argentina). *In*: H. Parent, G. Meléndez & F. Olóriz (*eds*.): Jurassic of South America. *Journal of South American Earth Sciences (Special Issue)* **16**: 143-165.

Parent H., Scherzinger A. & Schweigert G., 2006. The earliest ammonite faunas from the Andean Tithonian of the Neuqúen-Mendoza Basin, Argentina – Chile. *Neues Jahrbuch für Geologie und Paläontologie, Abhandlungen* **241**: 253-267.

Roman F., 1938. Les ammonites jurassiques et crétacées. Essai de genera. Masson, Paris, 554 p.

Schweigert G., Scherzinger A. & Parent H., 2002. The *Volanoceras* lineage (Ammonoidea, Simoceratidae) – a tool for long-distance correlations in the LowerTithonian. *Stuttgarter Beiträge zur Naturkunde* B**326**: 1-43.

Spath L.F., 1923-1943. A monograph of the Ammonoidea of the Gault. *Palaeontographical Society Monographs* **1-16**: 1-787.

Spath L.F., 1925. The Collection of fossils and rocks from Somaliland made by Messrs. B. N. K. Wyllie and W. R. Smellie. Part 7: Ammonites and aptychi. – *Monographs of the Geological Department of the Hunterian Museum* **1**: 111-164.

Spath L.F., 1927-1933. Revision of the Jurassic cephalopod faunas of Kachh (Cutch), India. *Geological Survey Memoirs, Palaeontographica Indica (new series)* **9(2)**: 1-945.

Uhlig V., 1903. Himalayan Fossils. The Fauna of the Spiti Shales. *Memoirs of the Geological Survey of Indica. Palaeontologica Indica, ser. 15*, **4(1)**: 1-132.

Verma H.M. & Westermann G.E.G., 1973. The Tithonian (Jurassic) Ammonite Fauna and Stratigraphy of Sierra Catorce, San Luis Potosi, Mexico. *Bulletin of American Paleontology* **63**/**277**: 107-320.

Yin J. & Enay R., 2004. Tithonian ammonoid biostratigraphy in eastern Himalayan Tibet. *Geobios* **37**: 667-686.

Wright C.W., Callomon J.H. & Howarth M.K., 1996. Volumen 4: Cretaceous Ammonoidea, Mollusca 4 (Revised), Part L. *In*: R.L. Kaesler (*ed*.): Treatise on Invertebrate Paleontology. The Geological Society of America and The University of Kansas: 1-362.

Zittel K.A. v., 1870. Die Fauna der älteren Cephalopoden führenden Tithonbildungen. *Palaeontographica Supplement* **1**: I-VII + 1-192.

Zittel K.A. v., 1884. Cephalopoda, p. 329-522. *In*: Zittel K.A. (*ed*.): Handbuch der Palaentologie, vol. 1, Abt. 2 (3); Munich & Leipzig (Oldenbourg).

Boletín
del Instituto de
Fisiografía y Geología

Recordatorio

Eliseo Popolizio

(19/04/1938 - 27/04/2008)

El día 27 de abril de 2008 ha fallecido el Dr.-Ing. Eliseo Popolizio.

Este destacado académico de la Universidad Nacional del Nordeste y de la Universidad Nacional de Rosario, especialista en Geomorfología y temas hídricos, se graduó como Ingeniero Civil en la Universidad Nacional de Rosario. Se formó en la investigación y en la docencia con Alfredo Castellanos y Pierina Pasotti, en el Instituto de Fisiografía y Geología; posteriormente fue becado para realizar estudios de posgrado en Geografía Física, en la Universidad de San Pablo, Brasil, con los profesores Ab´Saber y Bigarella.

Desde su primer trabajo de investigación publicado en 1963 publicó mas de 200 artículos científicos. Entre los trabajos mas destacados por sus colegas pueden citarse los dos informes publicados simultáneamente en 1975, con los nombre ¨Las redes de escurrimiento¨ y ¨Los sistemas de escurrimiento¨ (véase lista de referencias). Además realizó un gran número de trabajos de índole profesional.

Fue profesor en la cátedra Geología para Ingenieros en la Universidad Nacional de Rosario hasta que se trasladó en el año 1971 a la Facultad de Ingeniería de la Universidad Nacional del Nordeste. Allí organizó y dirigió el Centro de Geociencias Aplicadas, siendo a la vez profesor en las cátedras de Geomorfología (carrera de Geografía) y en Geología para Ingenieros y Fotointerpretación (carrera de Ingeniería Civil).

Dictó numerosas conferencias, fué docente de posgrado en distintas universidades y asistió a numerosos congresos nacionales e internacionales. Recibió un gran número de distinciones y premios, siendo designado en 1996 miembro de número de la Academia Nacional de Geografía. En 2003 obtuvo su Doctorado en Geografía en la Universidad del Salvador (Buenos Aires).

Su labor trascendió los claustros, ya que hace 29 años organizó y dirigió el Instituto Correntino del Agua (ICA) y posteriormente entre los años 1984 y 1987, se desempeñó como Subsecretario de Recursos Hídricos del Gobierno de la provincia de Corrientes.

Como profesional y ciudadano siempre preocupado por los problemas del desarrollo y crecimiento de su provincia, ocupaba actualmente la presidencia del Centro de Ingenieros de Corrientes.

Por último, cabe recordar que fue uno de los primeros socios de la Asociación Argentina de Geología Aplicada a la Ingeniería (ASAGAI).

SELECCIÓN DE PUBLICACIONES CIENTÍFICAS

Popolizio E., 1963. Un problema de Geomorfología Aplicada en la provincia de Corrientes. *Publicación de la Facultad de Ciencias Exactas, Ingeniería y Arquitectura, Universidad Nacional del Litoral* **39**.

Popolizio E., 1966. Sobre algunos rasgos estructurales del centro-sur de la Provincia de Corrientes. *Revista Univeristaria Lambda* **9-10**.

Popolizio E., 1966. Causas geográficas de los desplomes y deslizamientos de las riberas del Río Paraná y en especial en la ciudad de Corrientes. *Revista Univeristaria Lambda* **6-7**.

Popolizio E., 1967. Problemas geomorfoclimáticos en la Provincia de Corrientes. *27° Semana de Geografía, Sociedad Argentina de Estudios Geográficos (Buenos Aires)*.

Popolizio E. & Canoba C., 1968. Estudio aerofotográfico de paleopotamología en un sector ribereño del Río Paraná, Provincia del Chaco. *Notas del Instituto de Fisiografía y Geología* **A2**.

Popolizio E., 1969. Tentativa de contacto de cuencas sedimentarias con las áreas cristalinas del Brasil y la Argentina. *Anais do 23° Congreso Brasileiro de Geología, Bahía, Brasil*.

Popolizio E., 1970. Algunos rasgos de la geomorfología del Nordeste Argentino. *Boletín de la Sociedad Argentina de Botánica* **11**.

Popolizio E., 1972. La localización de paleopavimentos como yacimientos de materiales de construcción para carreteras. *Geociencias* **4(4)**.

Popolizio E., 1972. Geomorfología del relieve de

plataforma de la Provincia de Misiones y zonas aledañas. *Anales de la Sociedad Argentina de Estudios Geográficos* **15**: 17-84.

Popolizio E., 1973. Algunas vinculaciones entre la Geomorfología y los estudios hidrológicos. *Anales del Sexto Congreso Nacional del Agua (Comité Permanente de los Congresos Nacionales del Agua)* **1**.

Popolizio E., 1975. Carta Geomorfologica da area Jacareí, Santa Branca. *Centro de Geociencias Aplicadas UNNE* **12**.

Popolizio E., 1975. Los sistemas de escurrimiento. *Centro de Geociencias Aplicadas UNNE* **2**.

Popolizio E., 1975. Las redes de escurrimiento. *Centro de Geociencias Aplicadas UNNE* **2**.

Popolizio E., 1975. Contribución a la Geomorfología de la Provincia de Corrientes. *Notas del Instituto de Fisiografía y Geología* **A7-8**.

Popolizio E. & Serra P.Y., 1977. Fotointerpretación Aplicada al estudio de la Cuenca del Río Negro Provincia del Chaco. *Centro de Geociencias Aplicadas UNNE* **C14**.

Popolizio E., 1978. Génesis y evolución de la redes fluviales del Chaco Oriental. *Actas del Séptimo Congreso Geológico Argentino, Neuquén* **2**.

Popolizio E., Serra P.Y. & Hortt G., 1978. Bajos Submeridionales. Grandes unidades taxonómicas de Santa Fe. *Centro de Geociencias Aplicadas UNNE* **C7**.

Popolizio E., 1980. La teledetección como apoyo a la neotectónica del Nordeste Argentino. *Actas 26º Congreso Internacional de Geología, Paris, Sección 11*, Tema **12**.

Popolizio E., 1980. Fotointerpretación aplicada al estudio de las cuencas de la provincia del Chaco, situadas entre el límite sur de la cuenca del río Bermejo hasta aproximadamente los 25º30' Lat. Sur los 60º30' Long. Oeste, límite NE de la cuenca del río Negro y los ríos Paraguay y Paraná. *Publicaciones del Centro de Geociencias Aplicadas de la UNNE* **15(1)**.

Popolizio E., 1980. Los antiguos cauces del río Paraná de Corrientes a Esquina. *Centro de Geociencias Aplicadas de la UNNE* **13(6)**.

Popolizio E., 1980. La geomorfología en los estudios ecológicos de la llanura. *Centro de Geociencias Aplicadas de la UNNE* **11**.

Popolizio E. & Serra P.Y., 1980. Bases fisiográficas para el estudio de las crecientes e inundaciones en la Mesopotamia Argentina. *Centro de Geociencias Aplicadas UNNE* **C15(2)**

Popolizio E. & Serra P.Y. , 1980. La Geomorfología en los estudios ecológicos de la llanura. *Geociencias* **9**.

Popolizio E., Serra P.Y. & Hortt G., 1980. Bajos Submeridionales. Grandes unidades taxonómicas del Chaco. *Centro de Geociencias Aplicadas UNNE* **C3**.

Popolizio E., Borfitz A. & Serra P., 1980. Fotointerpretación aplicada al estudio de las causas de los desmoronamientos de ribera en la localidad de Lavalle (Provincia de Corrientes). *Centro de Geociencias Aplicadas UNNE* **C15(3)**.

Popolizio E., 1982. Geomophology of the Argentine Northeast. *Water International* **7**.

Popolizio E., 1983. Teoría General de Sistemas Aplicada a la Geomorfología. *Geociencias* **9**.

Popolizio E., 1983. La biorexistasia como método de datación relativa en las llanuras del nordeste argentino. *Geociencias* **11**.

Popolizio E., 1984. Influencia del sistema geomorfológico en las crecientes e inundaciones del Nordeste Argentino. *Geociencias* **14**.

Popolizio E., 1985. Criterios para el análisis y manejo de las inundaciones en el Nordeste Argentino. *Proceedings of the Fifth World Congress on Water Resources, Burssels*.

Popolizio E. & Canoba C., 1986. A remote sensing methodological approach for applied Geomorphology mapping in plain areas. *Proceedings of the Seventh International Symposium on Remote Sensing for Resources Development and Enviromental Management* **Comission VII**.

Popolizio E., 1987. El enfoque sistémico de la enseñanza de la Geografía. *Boletín de la Sociedad Argentina de Estudios Geográficos* **106**.

Popolizio E., 1987. Estudio del Macrosistema Iberá. Cartografía Geomorfológica-Hidrográfica. *Geociencias* **18**.

Popolizio E., 1990. Sensores remotos aplicados al reconocimiento de los sistemas de escurrimiento. *Geociencias* **18**.

Popolizio E., 1996. Las unidades geomorfológicas del Nordeste Argentino. *Anales de la 57 Semana de Geografía, Sociedad Argentina de Estudios Geográficos*.

Popolizio E., 1997. La importancia de la Teoría de la Biorexistasia en los estudios de Geomorfología del NEA. *Anales de la Academia Nacional de Geografía* **21**.

Popolizio E., 1998. Influence de la geomorphologie sur les inondations du Nord East Argentinien". *Annals 8th Congress of the International Association of Engineering Geology and Environment. Vancouver, Canadá*.

Popolizio E., 1999. Risk of flood on the light of climatic Global Change in Northeastern Argentina. *An International Symposium on Engineering Geology, Hidrology and Natural Disasters with emphasis on Asia, Kathmandú*.

Popolizio E., 1999. El Paraná, un río y su historia geomorfológica. *Centro de Geociencias Aplicadas UNNE* **C19**: 1-194 (tomo 1), 1-175 (tomo 2).

Popolizio, E., 2000. La importancia de la geomorfología frente al cambio climático global en el Nordeste Argentino. *Revista de Geología Aplicada a la Ingeniería y al Ambiente* **14**.

Popolizio E., 2000. Uniformitarismo o catastrofismo en la Geomorfofisiología del NEA. *Anales de la Sociedad Argentina de Estudios Geográficos* **21**.

Popolizio E., 2000. Influencia de la Tectónica en la geomorfología del Nordeste Argentino. *Anales 21 Reunión Científica de la Asociación Argentina de Geofísicos y Geodestas, Rosario.*

C. C. Canoba
Rosario

F. Lattuca
Departamento de Ciencias Geológicas, FCEIA, Universidad Nacional de Rosario, Pellegrini 250, 2000 Rosario, Argentina.

Rosario, 25/10/2008

INSTRUCCIONES PARA LOS AUTORES

Texto: Los artículos deben estar escritos en Español o Inglés. Tres copias completas del manuscrito (incluyendo todas las ilustraciones) serán remitidas a los editores. El texto debe ser tipeado en una cara de hojas A4 (210 x 297 mm), doble interlineado y con un margen derecho amplio. Una vez que el artículo sea aceptado, y luego de las últimas correcciones, el texto debe enviarse, junto a todas las ilustraciones, en CD-Rom o DVD-Rom. Formatos para texto: ASCII (.txt), rich text format (.rtf), WordPerfect (.wp), ó Word (.doc). El título del artículo y la traducción al segundo idioma, el (los) nombre(s) del (los) autor(es) y las direcciones postal y electrónica deben colocarse en la primera página. El texto debe paginarse a partir de la página con el título. El título debe ser tan corto como sea posible, con indicación acerca del área geográfica tratada en el texto; en los artículos de estratigrafía y/o paleontología debe incluirse, si correspondiera, además la edad. Un resúmen conciso que condense todos los resultados obtenidos debe colocarse al comienzo del artículo, en castellano/español y su traducción al inglés o francés. La totalidad del texto debe escribirse en letras minúsculas, utilizando las mayúsculas sólo al principio de oraciones y para los títulos de capítulos. En el texto, las referencias serán como sigue: Aguirre (1984); Dommergues & Meister (1995); Dagys et al. (1989). Notas al pie no serán admitidas (siempre es posible incorporar información complementaria o aclaratoria en el cuerpo del texto). Solamente se admitirá el uso de unidades del Sistema Internacional. Los autores de artículos paleontolólgicos deben seguir las reglas de los Códigos Internacionales de Botánica y Zoología. Los tipos y los fósiles ilustrados deben ser registrados y depositados en una institución apropiada permanente, debiendo citarse los números y el nombre de dicha institución. Las abreviaturas para nuevos taxa deben ser n. gen., n. sp., etc. Los números de láminas y figuras que fueron originalmente expresados en números no arábigos deben ser transformados a arábigos. Ejemplos:

1873 *Aspidoceras Beckeri* n. sp.- Neumayr: 202, pl. 18: 3.
1925 *Garantiana conjugata* Quenstedt.- Bentz: 162, pl. 6: 5-6.

Lista de referencias bibliográficas: Debe ser exhaustiva y exclusiva de las citas en el texto. Los artículos citados se ordenarán alfabéticamente por el apellido del autor principal, y cronológicamente cuando se citen mas que un trabajo de un mismo autor. Las referencias a artículos de un mismo autor en el mismo año se distinguirán en el texto y en el listado de referencias por las letras a, b, etc.: Pasotti (1977a, 1977b). Ejemplos:

Teichert C., 1987. An early German supporter of continental drift. *Earth Sciences Review* **5(1)**: 134-136.

Arkell W.J., 1957. Jurassic ammonites. *In*: Arkell W.J., Kummel B. and Wright C.W.: Treatise on Invertebrate Paleontology, (L) Mollusca 4, R.C. Moore (*ed*.). *University of Kansas Press and Geological Society of America, Kansas and New York*, 22+490p.

Brillouin L., 1962. Science and information theory, 2nd ed., 347 p., *Academic Press*, New York.

Figuras: Todas las ilustraciones (dibujos, diagramas, fotografías) deben ser numeradas como figuras y citadas en el texto, ser independientes y estar identificadas por numeración correlativa, con una explicación concisa y precisa, en la lengua del texto y con una traducción a la segunda. Su emplazamiento en el cuerpo del texto debe ser sugerido en el margen izquierdo del texto. Todas las ilustraciones, incluyendo las fotos, deben ser de excelente calidad y estar preparadas para eventual copia directa por barrido digital (escaneado). Tamaño máximo, en el caso de página completa, 170 x 247 mm. No se aceptarán figuras o láminas que excedan el tamaño máximo ni láminas que requieran plegarse (véanse posibilidades abajo, en Material Suplementario Digital). Cuando sea necesario indicar escala se hará en forma tan precisa como sea posible en la explicación de la figura y si es posible con una barra en la figura. Cuando una figura incluya varias partes o ilustraciones, éstas deben ser designadas con letras mayúsculas subordinadas al número de figura. Los originales de las ilustraciones serán remitidas solamente una vez que el manuscrito haya sido aceptado. Las fotografías deben montarse en cartulina flexible blanca, y deben ser claras, contrastadas y en el mismo tono dentro de una misma figura. La numeración de las fotos dentro de cada figura se indicará solamente en una cubierta de papel transparente (la numeración definitiva será preparada por los editores). Los editores prestarán todo el asesoramiento necesario para que los autores puedan enviar sus figuras en forma digital. Las figuras una vez preparadas y en su versión final pueden enviarse en formato TIFF o BMP con una calidad no inferior a 600 dpi, en grises de hasta 16 bits o 1200dpi para blanco y negro.

Pruebas de imprenta: El autor recibirá un juego de pruebas. En el caso de artículos con mas de un autor, deberá indicarse a cual enviar las pruebas para corrección tipográfica. En general no se aceptarán cambios ni agregados una vez confeccionadas las pruebas. Las pruebas de imprenta deben ser devueltas dentro de los 15 días posteriores a la recepción para asegurar la continuidad del proceso de edición. En caso de no devolución o devolución atrasada, los editores procederán con la revisión y eventuales correcciones.

Separatas: Se entregarán 50 separatas sin cargo al autor.

Envío de manuscritos: siguiendo las pautas listadas a

Instituto de Fisiografía y Geología
Boletín IFG
FCEIA - UNR
Pellegrini 250
2000 Rosario, Argentina

Material suplementario digital (MSD): Los autores pueden incluir suplementariamente, en forma digital, información y datos adicionales pertinentes al contenido de cada artículo publicado. Este material suplementario digital estará disponible en la página web del Boletín IFG: www.fceia.unr.edu.ar/fisiografia/publicaciones.htm. Podrán incluirse como MSD:

- Figuras en color y/o tamaños que superen el de la revista impresa 210 x 297 mm (formatos sugeridos: mapas de bits *.tif, *.bmp, *.eps; *.pdf).
- Grandes tablas numéricas o listados (formatos sugeridos: *.xls, *.doc, *.pdf).
- programas informáticos (enviar comprimidos: *.zip ó *.rar).
- listados de literatura publicada y/o inédita, no referida en el texto del artículo publicado (formato sugerido: *.pdf, *.doc, *.txt).

El MSD debe enviarse en CD-Rom o DVD-Rom, junto con el manuscrito según las instrucciones para autores; los editores evaluarán la posibilidad de su publicación y decidirán el formato definitivo de cada uno de los archivos.

El MSD no puede estar referido en el texto, el cual debe ser completamente autónomo del material suplementario.

Los autores deberán aceptar, por medio de la firma de una planilla específica, la posibilidad de discontinuidad temporaria o permanente de la página web del Boletín IFG o bien de partes de sus contenidos.

Boletín del Instituto de Fisiografía y Geología
ISSN 1666-115X

Volúmen 78, Números 1-2

Rosario - Diciembre 2008

Contenido / Contents